

Fast-weight Product Key Memory

Tianyu Zhao¹ and Llion Jones¹

¹Sakana AI

Sequence modeling layers in modern language models typically face a trade-off between storage capacity and computational efficiency. While softmax attention offers unbounded storage at prohibitive quadratic cost, linear variants are more efficient but suffer from limited, fixed-size storage. We introduce Fast-weight Product Key Memory (FwPKM), a sparse fast-weight memory layer that resolves this tension. FwPKM updates sparsely activated parameters at both training and inference time using chunk-level gradient descent on a local memory-rewrite objective. This performs Test-Time Training (TTT)-style gradient updates on activated slots in a sparse memory, enabling rapid memorization and retrieval of many new key-value associations while keeping per-token compute low and fixed. Experiments show that FwPKM functions as an effective episodic memory that complements the semantic memory of standard modules, yielding significant perplexity reductions on long-context datasets. Notably, in Needle-in-a-Haystack evaluations, FwPKM generalizes to 128K-token contexts despite being trained on only 4K-token sequences.

 **Code** <https://github.com/SakanaAI/fast-weight-product-key-memory>

Contents

1	Introduction	2
2	Preliminary	3
3	Fast-weight Product Key Memory	4
4	Experiments	6
5	Interpretability Analyses	12
6	Cost Analyses	14
7	Related Work	15
8	Conclusion	17
A	FwPKM Implementation Details	22
B	Pseudo Code	24
C	Detailed Experiment Settings	25
D	Ablation Study	27
E	More Visualization Examples	32

1. Introduction

Long-context language modeling often requires remembering specific, local facts (e.g. a name, a variable binding, a constraint) introduced tens of thousands of tokens earlier, and retrieving them when needed. The core sequence modeling layers, or token mixers, can be viewed as *associative memory* systems (Behrouz et al., 2025c; Dao and Gu, 2024; Gu and Dao, 2024; Peng et al., 2025; Sun et al., 2025; Vaswani et al., 2017; Yang et al., 2024b, 2025). In this framework, information from past tokens is encoded into storage (*i.e.* the process of *memorization*) and later integrated into a prediction step by querying that storage (*i.e.* the process of *retrieval*).

The current landscape is defined by a trade-off between memory capacity and computational efficiency. Softmax self-attention (Vaswani et al., 2017; Zhong et al., 2025) *memorizes* by explicitly storing a key-value pair for every past token and *retrieves* by comparing the current query to all stored keys, producing a weighted sum of values. This yields high-fidelity retrieval but at quadratic cost with sequence length. In contrast, modern Recurrent Neural Networks (RNNs) such as linear attention (Katharopoulos et al., 2020), Mamba2 (Dao and Gu, 2024), and DeltaNet (Schlag et al., 2021a; Yang et al., 2024b) compress history into a fixed-size state using learned update rules (e.g., Hebbian-style accumulation or Delta-rule error correction) and retrieve via a state readout in the form of vector–matrix multiplication. While this enables efficient, sub-quadratic retrieval, the fixed state capacity inherently limits the depth of information the model can retain compared to softmax attention.

To address the capacity limitations of these modern RNNs, recent work on Test-Time Training (TTT, Sun et al. 2025; Zhang et al. 2025b) and Titans (Behrouz et al., 2025c) replaces the fixed state matrix with a “fast-weight” (Hinton and Plaut, 1987; Schmidhuber, 1992) neural network (typically an MLP). Similar to a state matrix, this MLP adapts to input sequences on-the-fly by minimizing a reconstruction loss. However, these approaches face a scaling bottleneck: dense network structure. An MLP’s computation scales linearly with its parameter count. To store the massive amount of information required for long-context tasks, the fast-weight MLP must be large; yet, updating and querying a large, dense MLP frequently is computationally infeasible.

In this paper, we show that sparse associative memory offers a way around this constraint. Sparse memory architectures such as Product Key Memory (PKM, Lample et al. 2019) can maintain a very large number of memory parameters while activating only a small subset per token. We introduce Fast-weight Product Key Memory (FwPKM), which transforms PKM from a static, slow-weight module into a dynamic fast-weight episodic memory. By redesigning the sparse memory to update its key/value matrices via gradient descent at inference time, we enable FwPKM to memorize vast amounts of context with fixed per-token compute. This distinction allows us to conceptually separate memory roles: standard slow weights serve as *Semantic Memory* (storing dataset-wide facts), while FwPKM serves as *Episodic Memory* (storing context-specific bindings).

Our main contributions are threefold.

- **Architecture.** We introduce Fast-weight Product Key Memory (FwPKM), a new sequence modeling layer that enables “Sparse Test-Time Training” – TTT-style gradient updates over a *sparse* memory. We detail the architectural modifications and optimization objectives required to make sparse fast weights stable and effective (Section 3).
- **Performance.** We demonstrate that FwPKM acts as a robust episodic memory when plugged into hybrid backbones. In Needle-in-a-Haystack evaluations, FwPKM generalizes to 128K-token contexts despite being trained on only 4K sequences, with iterative reading boosting retrieval accuracy from < 10% to > 70% (Section 4.3). FwPKM also consistently reduces perplexity on long-context datasets like LC64 and Longbench (Section 4.2, 4.4). Furthermore, we analyze continual learning capabilities, finding that while the model adapts to new domains online, it

faces challenges with retention, motivating future work in memory consolidation (Section 4.5).

- **Analysis.** We provide interpretability analyses showing that FwPKM explicitly captures informative entities and novel patterns (Section 5), alongside a cost analysis highlighting where sparse memory helps and where faster kernels are needed for broader scaling (Section 6).

2. Preliminary

We briefly review sparse key-value memories and Product Key Memory (PKM, Lample et al. 2019), which we later extend into an online-updated fast-weight module.

2.1. Sparse Top- k key-value memory

A standard key-value memory consists of a key matrix $K \in \mathbb{R}^{N \times d_k}$ and a value matrix $V \in \mathbb{R}^{N \times d_v}$, where N is the number of memory slots and $d_{\{k,v\}}$ are the hidden dimensions. Given a query vector $\mathbf{q} \in \mathbb{R}^{d_k}$, the model scores each slot (e.g., via dot product),

$$s_i = \mathbf{q}^\top K_i, \quad (1)$$

selects the indices of the Top- k scores \mathcal{I} ,

$$\mathcal{I} = \text{Top-}k(\{s_i\}_{i=1}^N). \quad (2)$$

Then it computes normalized scores $\{s'_i\}$ via softmax,

$$\{s'_i\} = \text{softmax}(\{s_j\}_{j \in \mathcal{I}}), \quad (3)$$

and retrieves a weighted sum of values,

$$\hat{\mathbf{v}} = \sum_{i \in \mathcal{I}} s'_i V_i. \quad (4)$$

Top- k sparsity reduces the number of *accessed* value rows, but still requires *scoring* all N keys to identify the top candidates. This linear $O(N)$ complexity prohibits scaling to massive memory sizes (e.g. $N \approx 10^6$).

2.2. Product Key Memory (PKM)

Product Key Memory (Lample et al., 2019) reduces the *scoring* cost by factorizing the keys into two smaller codebooks. PKM splits the query into two sub-queries $\mathbf{q} = [\mathbf{q}^{(1)}; \mathbf{q}^{(2)}]$, where $\mathbf{q}^{(1)}, \mathbf{q}^{(2)} \in \mathbb{R}^{d_k/2}$, and maintains two sub-key matrices $K^{(1)}, K^{(2)} \in \mathbb{R}^{\sqrt{N} \times d_k/2}$. It scores each codebook independently,

$$s_i^{(1)} = \mathbf{q}^{(1)\top} K_i^{(1)}, \quad s_j^{(2)} = \mathbf{q}^{(2)\top} K_j^{(2)}, \quad (5)$$

selects Top- k indices for each codebook,

$$\mathcal{I}^{(1)} = \text{Top-}k(\{s_i^{(1)}\}_{i=1}^{\sqrt{N}}), \quad \mathcal{I}^{(2)} = \text{Top-}k(\{s_j^{(2)}\}_{j=1}^{\sqrt{N}}), \quad (6)$$

and then searches over the restricted Cartesian product $\mathcal{I}^{(1)} \times \mathcal{I}^{(2)}$ using additive pairwise scores

$$s_{i,j} = s_i^{(1)} + s_j^{(2)}, \quad (i, j) \in \mathcal{I}^{(1)} \times \mathcal{I}^{(2)}. \quad (7)$$

Finally, PKM selects the Top- k pairs from this restricted set, applies softmax over the selected pair scores, and retrieves from the corresponding rows of the value table $V \in \mathbb{R}^{N \times d_v}$, where 1-indexed pair (i, j) maps to row $((i-1) \times \sqrt{N} + j)$.

This decomposition of key space yields an efficient Top- k retrieval that avoids scoring all N slots. It allows PKM to index millions of slots (e.g., 10^6) using only thousands of scores (2×10^3), making it an ideal choice for high-capacity associative memory.

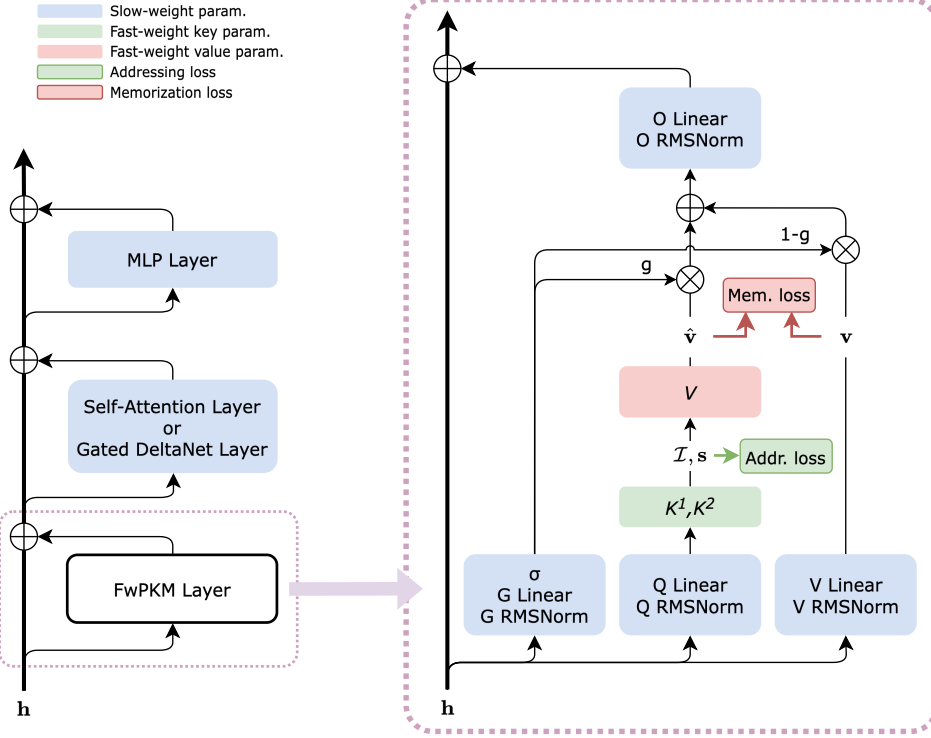


Figure 1 | **Architecture of FwPKM.** An FwPKM layer is placed before a token mixer (*i.e.* a self-attention or a Gated DeltaNet layer). **Slow-weight parameters** are updated at only training time, using a global language modeling loss. **Fast-weight value parameters** and **key parameters** are updated at both training and inference time, by minimizing local **memorization loss** and **addressing loss**, respectively.

3. Fast-weight Product Key Memory

Standard Product Key Memory (PKM) is a **slow-weight** sparse channel mixer, meaning that its parameters are learned by the global language modeling objective over a corpus and then remain frozen at inference. As a result, PKM mainly stores *semantic* knowledge but cannot rapidly incorporate *episodic* information from the current input stream. We propose **Fast-weight Product Key Memory** (FwPKM), which keeps PKM’s **retrieval process unchanged**, but redesigns the **memorization process** by updating the memory matrices online. Concretely, FwPKM stores key-value associations from the input sequence by minimizing a local reconstruction objective over chunks, in the spirit of test-time training.

3.1. Overview

Figure 1 summarizes FwPKM. Given hidden states $\mathbf{h}_{1:T}$ ¹, we process them in chunks of size C . Within each chunk, FwPKM: (i) **constructs** query/value vectors and a scalar gate using slow-weight projections, (ii) **retrieves** a sparse value prediction with PKM using the current fast weights, and (iii) **writes** to the fast weights by optimizing local objectives over the chunk. Concretely, we update the value matrix V by minimizing a gated reconstruction loss \mathcal{L}_{mem} (Section 3.3), and update the key matrices K^1, K^2 by minimizing an auxiliary addressing loss $\mathcal{L}_{\text{addr}}$ that prevents slot collapse (Section 3.4). We apply these fast-weight updates after processing the chunk, so predictions within the chunk depend only on the fast weights from previous chunks, preserving causality.

¹We abuse tensor subscripts to index both sequence and feature dimensions; t indexes sequence position and i, j index feature dimensions.

3.2. Forward Pass: Inputs and Retrieval

Input construction. For each token t , a slow-weight network parameterized by ϕ constructs inputs to FwPKM:

$$\mathbf{q}_t = \text{Linear}_\phi^q(\text{RMSNorm}_\phi^q(\mathbf{h}_t)), \quad (8)$$

$$\mathbf{v}_t = \text{Linear}_\phi^v(\text{RMSNorm}_\phi^v(\mathbf{h}_t)), \quad (9)$$

$$g_t = \sigma\left(\text{Linear}_\phi^g(\text{RMSNorm}_\phi^g(\mathbf{h}_t))\right). \quad (10)$$

where $\mathbf{q}_t \in \mathbb{R}^{d_k}$, $\mathbf{v}_t \in \mathbb{R}^{d_v}$, $g_t \in (0, 1)$ and $\sigma(\cdot)$ denotes the sigmoid function.

Sparse retrieval. FwPKM uses the same product-key sparse retrieval as PKM (Section 2.2). Given \mathbf{q}_t , PKM returns a sparse index set \mathcal{I}_t and normalized weights $\{s'_{t,i}\}_{i \in \mathcal{I}_t}$, and predicts a value by a weighted sum of value rows:

$$\hat{\mathbf{v}}_t = \text{PKM}(\mathbf{q}_t; \theta) = \sum_{i \in \mathcal{I}_t} s'_{t,i} V_i. \quad (11)$$

Gated Residual Output. Next-token prediction does not always require episodic memory, so we interpolate the retrieved value with a residual value path:

$$\mathbf{o}_t = g_t \cdot \hat{\mathbf{v}}_t + (1 - g_t) \cdot \mathbf{v}_t, \quad \mathbf{o}'_t = \text{Linear}_\phi^o(\text{RMSNorm}_\phi^o(\mathbf{o}_t)). \quad (12)$$

3.3. Backward Pass: Memorization by Learning to Reconstruct

Chunk-level local objective. Within each chunk, FwPKM updates fast weights θ to make retrieval reconstruct target values derived from the same stream. Following TTT-style fast weights, we minimize a reconstruction loss over query-value pairs. For a chunk of size C , define

$$\mathcal{L}_{\text{mem}} = \sum_{t=1}^C \frac{1}{2} g_t \|\mathbf{v}_t - \hat{\mathbf{v}}_t\|_2^2. \quad (13)$$

Why MSE and the $\frac{1}{2}$ factor. The MSE gradient provides an explicit “rewrite” signal. For a single prediction-target pair $(\hat{\mathbf{v}}, \mathbf{v})$, the gradient with respect to the prediction is $\nabla_{\hat{\mathbf{v}}} \frac{1}{2} \|\mathbf{v} - \hat{\mathbf{v}}\|_2^2 = -(\mathbf{v} - \hat{\mathbf{v}})$. Thus, if we could update the prediction directly, a unit step would rewrite it to the target: $\hat{\mathbf{v}} \leftarrow \hat{\mathbf{v}} - \nabla_{\hat{\mathbf{v}}} = \mathbf{v}$. In FwPKM we do not update $\hat{\mathbf{v}}$ directly; instead we update the underlying value rows V_i that produced $\hat{\mathbf{v}}$. Nevertheless, the same residual term $(\mathbf{v} - \hat{\mathbf{v}})$ acts as the update signal, making the fast-weight update behave like explicit memory rewriting.

Gradient aggregation. Multiple tokens in a chunk may write to the same value row. Let N_i^{read} denote the number of times row V_i is accessed in the chunk. We aggregate per-row gradients by normalizing with N_i^{read} . This aggregation works as a consensus mechanism for competing memory writings.

$$\nabla_{V_i}^{\text{agg}} = \frac{1}{N_i^{\text{read}}} \nabla_{V_i} \mathcal{L}_{\text{mem}}. \quad (14)$$

For the memorization, we use $\nabla_{V_i}^{\text{agg}}$ to update the accessed value rows:

$$V_i \leftarrow V_i - \nabla_{V_i}^{\text{agg}}. \quad (15)$$

3.4. Backward Pass: Prevent Slot Collapsing via Addressing Optimization

Sparse memories can suffer from *memory slot collapsing*, where only a small fraction of slots are used. We therefore optimize an auxiliary addressing objective that encourages balanced slot usage on average across a chunk, without forcing each individual query to be uniform.

Let $\mathbf{s}'_t{}^1 \in \mathbb{R}^{\sqrt{N}}$ and $\mathbf{s}'_t{}^2 \in \mathbb{R}^{\sqrt{N}}$ be the normalized Top- k score vectors over the two sub-key sets (unselected indices have score 0). Define marginal slot-usage distributions as:

$$\bar{\mathbf{p}}^1 = \frac{1}{C} \sum_{t=1}^C \mathbf{s}'_t{}^1, \quad \bar{\mathbf{p}}^2 = \frac{1}{C} \sum_{t=1}^C \mathbf{s}'_t{}^2, \quad (16)$$

and minimize $\mathcal{L}_{\text{addr}}$ which is the negative entropy:

$$\begin{aligned} \mathcal{L}_{\text{addr}} &= -H(\bar{\mathbf{p}}^1) - H(\bar{\mathbf{p}}^2) \\ &= -\sum_{i=1}^{\sqrt{N}} \bar{p}_i^1 \log \bar{p}_i^1 - \sum_{i=1}^{\sqrt{N}} \bar{p}_i^2 \log \bar{p}_i^2. \end{aligned} \quad (17)$$

We update keys using the gradients of $\mathcal{L}_{\text{addr}}$:

$$K^1 \leftarrow K^1 - \nabla_{K^1} \mathcal{L}_{\text{addr}}, \quad K^2 \leftarrow K^2 - \nabla_{K^2} \mathcal{L}_{\text{addr}}. \quad (18)$$

3.5. Practical Choices

We found the following choices helpful for improving model performance and training stability. Detailed discussion and ablations are deferred to Appendix A and Appendix D, respectively.

- **Lookahead value targets.** During memorization, we pair \mathbf{q}_t with \mathbf{v}_{t+1} . In this way, a query extracts information about the immediate future of similar queries in history, which aligns the local reconstruction task with the global next-token prediction task (Appendix A.1).
- **IDW scoring.** Instead of scoring a key row by dot product $\mathbf{q}^{(m)\top} K_i^{(m)}$, $m \in \{1, 2\}$ (Eq. 5), we use an inverse-distance weighting (IDW, McCarter 2023) score that depends on Euclidean distance, which encourages keys to become *clustering centroids* in representation space. We apply IDW by changing the scoring function from $\mathbf{q}^\top K_i$ to $-\log(\epsilon + \|\mathbf{q} - K_i\|_2^2)$ (Appendix A.2).
- **Target normalization.** We z-score normalize \mathbf{v}_t along the feature dimension for stability (Appendix A.3).

4. Experiments

We evaluate FwPKM along four axes. First, we use perplexity on short- and long-context corpora to disentangle **semantic** (slow-weight) and **episodic** (fast-weight) memory roles. Next, we stress-test episodic retrieval with Needle-in-a-Haystack, including **iterative rereading** that leverages test-time optimization. Finally, we evaluate on realistic long-context QA tasks from LongBench and probe **online domain adaptation** on diverse Pile subsets.

4.1. Training Setting

Model We implement 12-layer language models that follow the QwenNext design principles (Qwen Team, 2025a,b) but are scaled down to our setting (baseline models are $\sim 112\text{M}$ parameters), interleaving Gated DeltaNet (GDN, Yang et al. 2025) and gated softmax attention layers (Qiu et al., 2025). Our investigation uses the following baseline configurations.

- GDN: Gated DeltaNets at all 12 layers

- GDN+SWA: GDN interleaved with Sliding Window Attention (SWA, window size 512) at a 3:1 ratio
- GDN+FA: GDN interleaved with Full Attention (FA) at a 3:1 ratio
- FA: Full Attention at all layers

We introduce PKM and FwPKM modules into these baselines at specific depths (layers 2, 6, and 10). A standard PKM layer replaces the original MLP, while an FwPKM layer is inserted before the token mixer (Attention/GDN). Both PKM and FwPKM have 512^2 memory slots (262,144). PKM retrieves effectively Top-128 slots (4 heads and 32 slots per head) while FwPKM retrieves Top-8 slots (1 head and 8 slots per head). We choose 8 slots because it hits a balance between efficiency and performance. See ablation experiments in Appendix D.

We further include two types of baselines. For the first kind, we substitute the PKM architecture in FwPKM@2, 6, 10 with a SwiGLU MLP (Shazeer, 2020) that maintains three fast-weight matrices and their biases for up-/gating-/down-projection. This variant is denoted as FwMLP@2, 6, 10. In addition, we use LaCT (Zhang et al., 2025b) as the second baseline. LaCT is an improved TTT (Sun et al., 2025) model that uses a sliding window attention, a fast-weight SwiGLU MLP, and a slow-weight SwiGLU MLP in every layer. Its fast weights are updated using SGD+momentum with L2 weight normalization (Salimans and Kingma, 2016).

Data To incentivize the learning of cross-chunk dependencies via FwPKM, we use 5B tokens from LongContext64 (Buckman), a dataset consisting of long-context documents (> 64K tokens) sourced from RedPajama V2 (Weber et al., 2024). We supplement this with 5B tokens from Fineweb-Edu (Penedo et al., 2024) to maintain high-quality language modeling capabilities. All models are trained with a sequence length of 4K tokens.

We refer readers to Appendix C for more details of the architectures and optimization.

4.2. PPL Evaluation

We evaluate perplexity (PPL) on three distinct datasets to assess different memory capabilities: **Fineweb-Edu** (knowledge-intensive, short context), **LC64** (in-domain, long context), and **LAMBADA** (Paperno et al. 2016, out-of-domain, long context). Each evaluation dataset contains 8M tokens.

Evaluation protocol For PPL evaluation, we evaluate 4K-token sequences in their original order with a batch size of 1 so that segments are presented sequentially *without resetting* fast weights between adjacent segments. This enables fast weights to capture dependencies across segment boundaries. Figure 2 shows perplexities for all models.

Finding 1: FwPKM and PKM serve distinct, complementary roles. Baseline models with layouts GDN and GDN+SWA lack components for modeling long-range dependency, and their FwPKM versions address the weakness. As shown in Figure 2, FwPKM significantly reduces PPL on long-context datasets (LC64, LAMBADA), confirming its role as an **episodic memory**. In contrast, standard PKM provides the largest gains on Fineweb-Edu, acting as a **semantic memory** for general knowledge. The combination of both modules yields the best performance across all metrics, suggesting they address orthogonal limitations in the baseline architectures. In Appendix D.2 and E.1, we further demonstrate that FwPKM is likely to exploit cross-sequence dependency to reduce PPL on long-context datasets.

Finding 2: FwPKM competes with Full Attention. When FwPKM is added to baselines with unrestricted Full Attention (FA and GDN+FA), PPL improvements are marginal. Analysis of gating

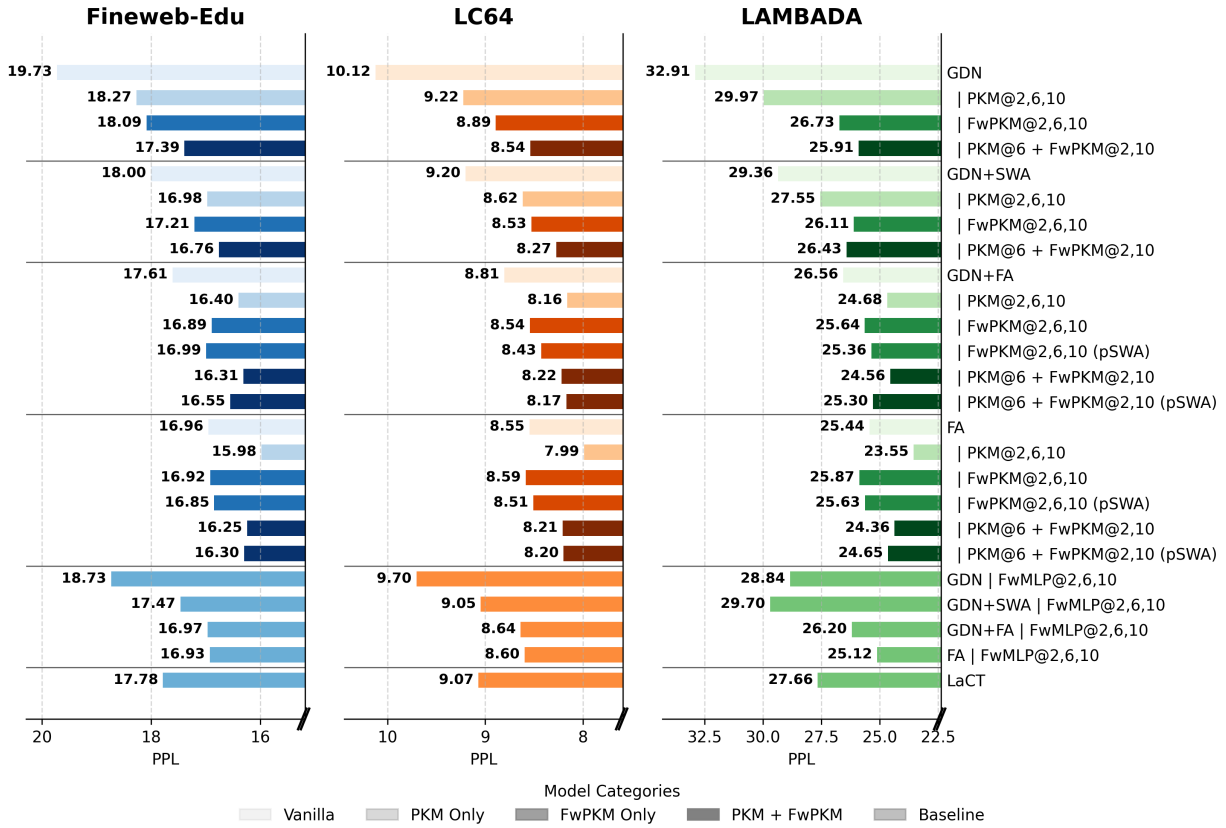


Figure 2 | Perplexity on Fineweb-Edu, LC64, and LAMBADA. We use bar colors to help distinguish between models with different types of memory components.

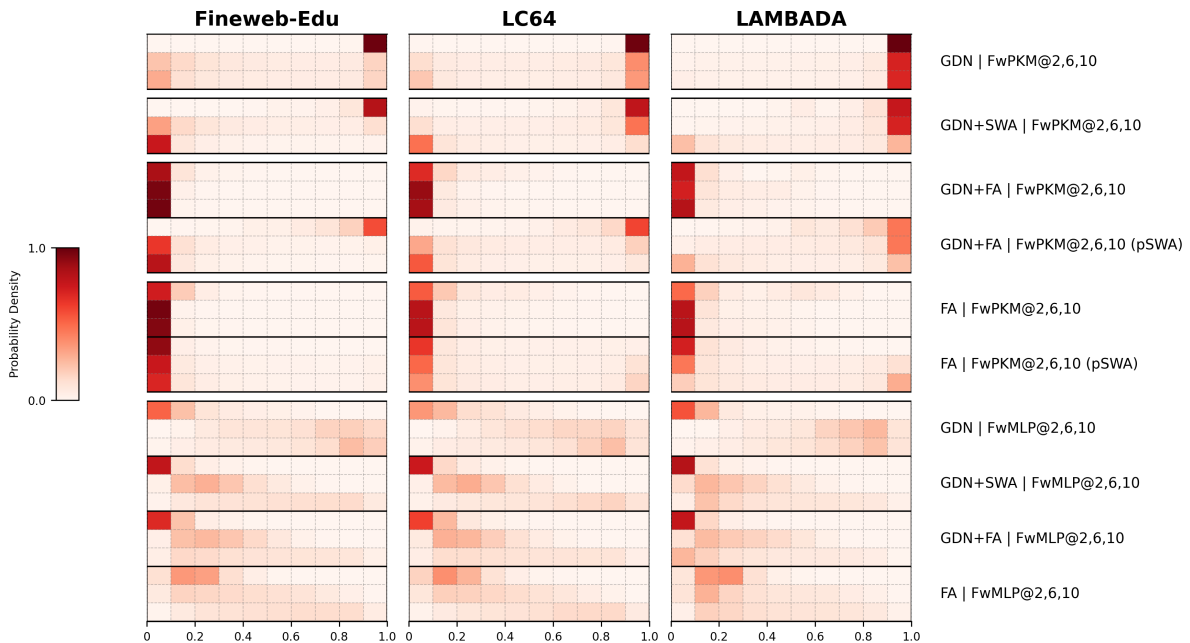


Figure 3 | FwPKM gating value distribution on Fineweb-Edu, LC64, and LAMBADA test sets. Each row represents one FwPKM layer. The probability densities are categorized into 10 bins. A darker color suggests a higher probability density of a bin.

values in Figure 3 reveals that these models learn to ignore FwPKM, with gating weights clustering near zero.

Finding 3: Restricting full attention facilitates FwPKM use. To mitigate the above issue, we restrict full attention’s long-range perception at *training time* by imposing a sliding attention window of length 512 on all full attention layers with probability 0.9. Denoted by a suffix pSWA, these models learn to use FwPKM more, as suggested by increased high-end mass in the gating distributions in Figure 3. While pSWA has minimal impact on PPL, we will see a more significant difference in the following experiments.

4.3. Needle-in-a-Haystack Evaluation

We conduct Needle-in-a-Haystack (NIAH, Kamradt 2023; Mohtashami and Jaggi 2023) evaluation to further verify FwPKM’s functionality as episodic memory. In all NIAH experiments, we update fast weights after reading the full haystack (and after each *rereading* iteration, see below); we do not perform additional updates while generating the answer.

In the basic setting, we construct 500 NIAH samples from the LAMBADA dataset. Each sample contains a haystack – a 4K-length sequence from the LAMBADA dataset with 5 needles inserted at random positions, where each needle contains a unique 4-character key and a 6-digit value – and a question that requests the value of a specific key. To test FwPKM’s large memory storage, we additionally construct test sets of 8K, 32K, and 128K context lengths.

Iterative Memorization (n -iter NIAH). A unique feature of FwPKM is its ability to improve memory fidelity by re-processing the same input. We define a n -iter NIAH setting, where the model forwards the same haystack context n times before answering. FwPKM’s process chunk size C is accordingly changed to the length of each haystack context such that it updates its memory once after reading an entire haystack. The basic setting is 1-iter NIAH.

Accuracy results of n -iter NIAH ($n \in \{1, 2, 3, 4\}$) on the four test sets of 4K-128K context lengths are shown in Figure 4. The accuracies of all iterations are drawn as a stacked bar.

Finding 4: Iterative reading boosts retrieval accuracy. For GDN and GDN+SWA layouts, a single pass (1-iter) is often insufficient for perfect retrieval. However, a second pass (2-iter) yields a massive boost in accuracy (jumping from $< 10\%$ to $> 50\%$ in many cases). More passes further improve the accuracy to $> 70\%$. This confirms that FwPKM effectively exploits test-time training to consolidate episodic memories, surpassing softmax attention. In addition, effective iterative memorization (in Figure 4) correlates with high gating values (in Figure 3).

Finding 5: FwPKM generalizes to 128K contexts. Despite being trained on only 4K-token sequences, FwPKM generalizes effectively to 128K tokens. While FA baselines degrade rapidly on context lengths unseen during training, FwPKM maintains robust retrieval performance.

4.4. Longbench Evaluation

In addition to the synthetic NIAH task, we assess long-context modeling on realistic data from Longbench (Bai et al., 2024). Longbench contains 21 tasks whose average length ranges from 5K to 15K whitespace-separated words. The tasks are mostly question answering and summarization, but their generative nature makes it difficult for pretrained-only (non instruction-tuned) models to produce well-calibrated free-form answers. Instead of computing official metrics such as F1 score, we use perplexity for evaluation.

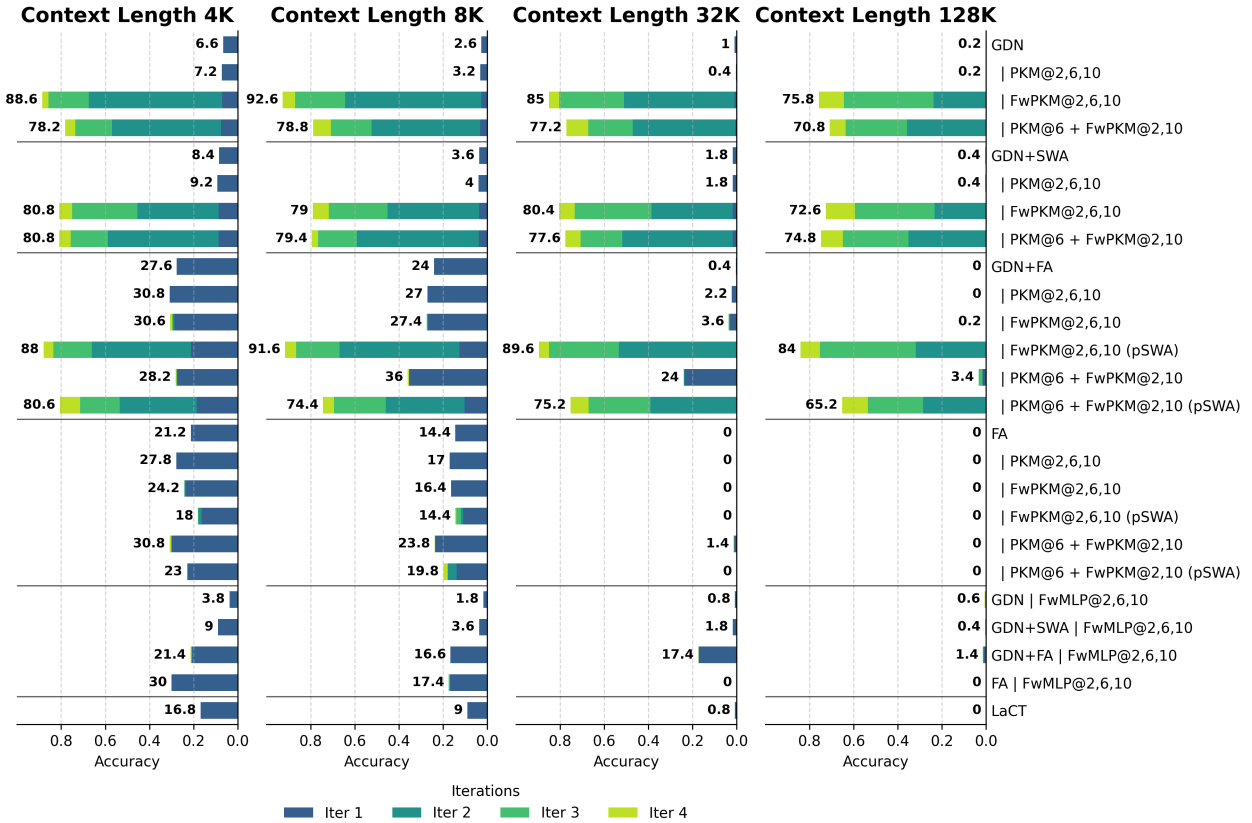


Figure 4 | Stacked bar plots for NIAH accuracy results on 4K-/8K-/32K-/128K-length test sets. Each stacked bar shows the accuracies of {1, 2, 3, 4}-iter NIAH evaluations.

We select *2WikiMultihopQA*, *HotpotQA*, *MultiFieldQA-en*, *MuSiQue*, and *NarrativeQA*, resulting in 950 examples with an average length of 17421 tokens and a maximum length of 81616 tokens. We only compute perplexity on answer tokens. For examples with multiple answer references, we use the first reference for perplexity computation. We update fast weights once after reading the entire context (i.e., no updates during answer generation), mirroring the 1-iter NIAH protocol. We omit the data for LaCT because it performs poorly on the Longbench data (PPL > 100).

Finding 6: FwPKM reduces answer-token perplexity on realistic long-context tasks. As shown in Figure 5, FwPKM effectively reduces perplexity on these long-context tasks for GDN, GDN+SWA, and GDN+FA models where FwPKM is actively utilized.

4.5. Continual Learning Evaluation

Beyond long-context modeling, we study whether the large-scale fast weights in FwPKM adapt to new data domains. We devise an *adapt-and-test* experiment. From the Pile corpus (Gao et al., 2020), we choose six subsets *DM Mathematics*, *FreeLaw*, *PhilPapers*, *PubMed Central*, *Ubuntu IRC*, and *USPTO Backgrounds* to represent different professional domains. For each domain, we sample a 4M-token *adapt set* and a 4M-token *eval set* without overlap.

We run 6 adaptation stages sequentially (one per domain’s *adapt set*), during which fast weights are updated while slow weights are frozen. After each adaptation stage, we compute the model’s average negative log-likelihood (NLL) on all 6 *eval sets* and report changes relative to the initial NLL before the first stage. In Figure 6, domains correspond to colors, used both for the background shading of each adaptation stage and for the lines showing Δ NLL.

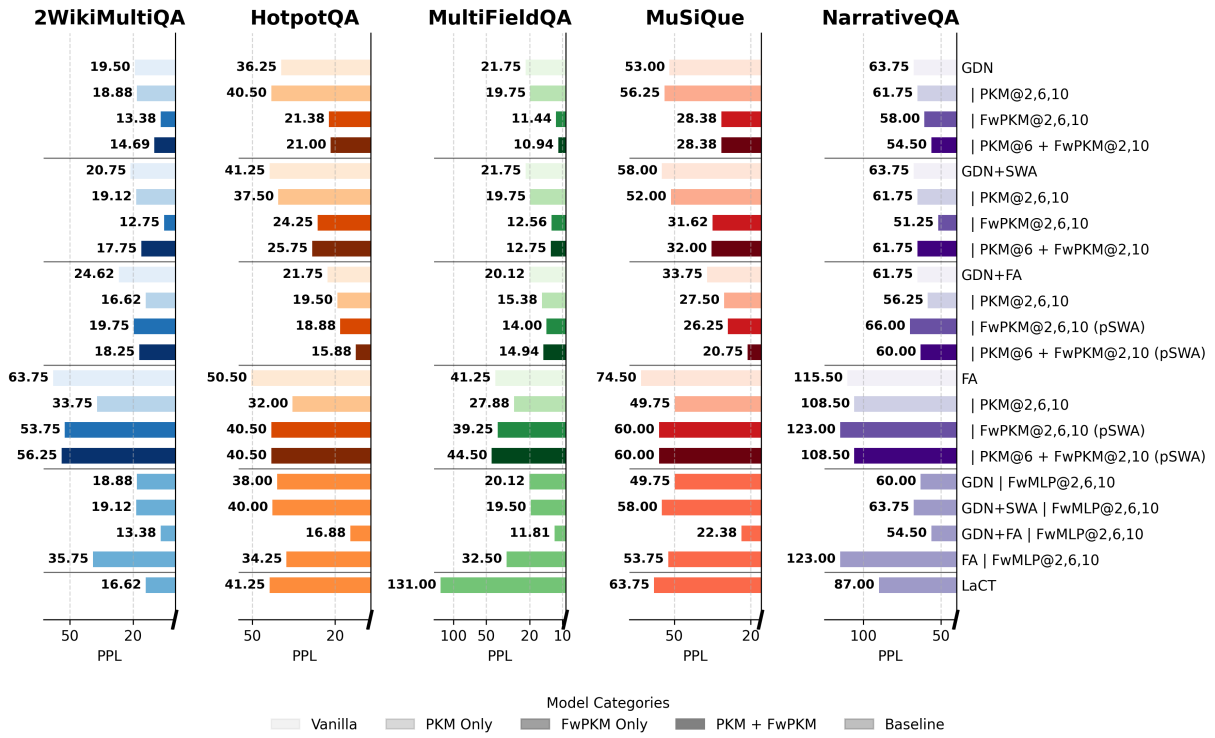


Figure 5 | Perplexity on five Longbench tasks. We use bar colors to help distinguish between models with different types of memory components.

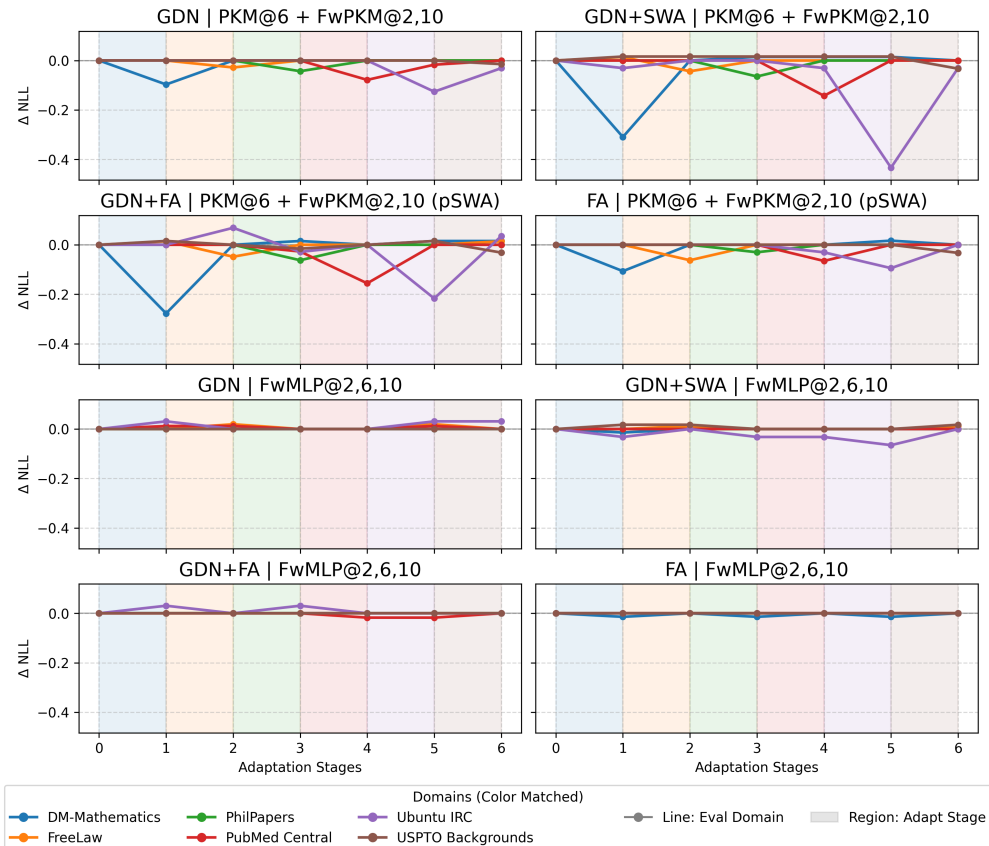


Figure 6 | Change of negative log-likelihood (ΔNLL) on six Pile domain datasets before and after 6 adaptation stages of test-time learning on each domain dataset.

Finding 7: FwPKM adapts quickly but struggles with retention across stages. As expected, after each adaptation stage, the NLL of the corresponding domain decreases as the fast weights store related domain knowledge. However, these gains often do not persist across subsequent stages, suggesting that previously stored fast-weight knowledge is flushed and replaced by newer domains. This motivates developing a memory retention mechanism to realize long-term continual learning in future work.

5. Interpretability Analyses

A key advantage of FwPKM over black-box architectures is its inherent interpretability. Because memory slots are explicitly written and read, we can trace retrieved information back to specific input tokens.

5.1. Case Study: Probing Memory in NIAH

We investigate the internal retrieval mechanism by visualizing the memory access patterns of the GDN+SWA|PKM@6+FwPKM@2,10 model during a 4-iter Needle-in-a-Haystack (NIAH) task with a 4K context. Specifically, we trace the model’s internal state as it generates the 6-digit passkey answer.

Figure 7 displays the Top-8 retrieved memory slots for both a lower layer (Layer 2) and a higher layer (Layer 10) at each generation step. For every retrieved slot, we decode and display the content stored during the latest memorization step: the **query token** (the key used for addressing), the **target value token** (the predicted next token), and the **surrounding context** (the text window surrounding the target in the original haystack). To facilitate analysis, we mark slots with a **[HIT]** label if they explicitly store the ground-truth next token required for the current generation step.

High-precision retrieval As shown in Figure 7, the majority of retrieved slots contain the correct target tokens associated with the query needle. The model successfully surfaces the specific needle (ID “8320” at depth 89.66%) from thousands of tokens, populating the top slots with the correct 6-digit value sequence (“964876”).

Robust aggregation Despite individual slot errors, the model successfully aggregates information across the 16 slots from the two FwPKM layers to generate the correct 6-digit value. This demonstrates that FwPKM functions as a robust distributed storage system, where consensus across multiple slots compensates for noise in individual retrievals.

5.2. Case Study: Selective Gating

We further examine the “gating values” g_t to understand when the model chooses to rely on episodic memory versus its static slow weights. To visualize this, we feed the Wikipedia article for “Sakana AI”²—a topic unseen during the model’s pre-training—into the network. We adjust the update chunk size from 512 to 32 to capture fine-grained local adaptivity.

Figure 8 presents a heatmap of the gating scalar g_t with input text in the foreground. Higher intensity (represented by darker bars) indicates a value of g_t closer to 1, signifying a strong reliance on the fast-weight episodic memory. Conversely, lower intensity indicates reliance on the pre-trained slow weights.

Layer specialization We observe distinct behaviors across model depths. The lower-layer FwPKM tends to maintain high gating values across almost all tokens, acting as a general-purpose buffer

²https://en.wikipedia.org/wiki/Sakana_AI

Needles

... ID-8320: 964876 ... ID-d83f: 645749 ... ID-97d9: 831209 ... ID-3ba3: 158393 ... ID-8fab: 099170 ...

Output Token 1: '9'

--- FwPKM Layer 2 ---

Slot 161817 | [HIT] | Q: | V in ctx:...D-8320 is 964876. cry...
 Slot 162216 | [HIT] | Q: | V in ctx:...D-8320 is 964876. cry...
 Slot 14361 | [HIT] | Q: | V in ctx:...D-8320 is 964876. cry...
 Slot 161945 | [HIT] | Q: | V in ctx:...D-8320 is 964876. cry...
 Slot 14760 | [HIT] | Q: | V in ctx:...D-8320 is 964876. cry...
 Slot 28697 | [HIT] | Q: | V in ctx:...D-8320 is 964876. cry...
 Slot 129049 | | Q: hand | V in ctx:...g one hand on top of th...
 Slot 162198 | [HIT] | Q: | V in ctx:...D-8320 is 964876. cry...

--- FwPKM Layer 10 ---

Slot 1506 | | Q: | V in ctx:...D-97d9 is 831209. a f...
 Slot 1064 | | Q: | V in ctx:...D-97d9 is 831209. a f...
 Slot 148962 | | Q:the | V in ctx:...pie-in-the-sky while ...
 Slot 148520 | | Q: bottl | V in ctx:...f a bottle of water . s...
 Slot 24034 | | Q: membe | V in ctx:...ior member of the leade...
 Slot 234978 | | Q: | V in ctx:...D-4ad4 is 512407. nev...
 Slot 175074 | | Q:using | V in ctx:...n accusing voice bit back ...
 Slot 108514 | | Q: | V in ctx:...D-7ff8 is 930401. set...

Output Token 2: '6'

--- FwPKM Layer 2 ---

Slot 26757 | [HIT] | Q:9 | V in ctx:...-8320 is 964876. cryi...
 Slot 28805 | [HIT] | Q:9 | V in ctx:...-8320 is 964876. cryi...
 Slot 27040 | [HIT] | Q:9 | V in ctx:...-8320 is 964876. cryi...
 Slot 26781 | [HIT] | Q:9 | V in ctx:...-8320 is 964876. cryi...
 Slot 159877 | [HIT] | Q:9 | V in ctx:...-8320 is 964876. cryi...
 Slot 27125 | [HIT] | Q:9 | V in ctx:...-8320 is 964876. cryi...
 Slot 26899 | [HIT] | Q:9 | V in ctx:...-8320 is 964876. cryi...
 Slot 135301 | [HIT] | Q:9 | V in ctx:...-8320 is 964876. cryi...

--- FwPKM Layer 10 ---

Slot 172940 | [HIT] | Q:9 | V in ctx:...-8320 is 964876. cryi...
 Slot 235404 | [HIT] | Q:9 | V in ctx:...-8320 is 964876. cryi...
 Slot 216972 | | Q:5 | V in ctx:...ffb2 is 253297. throu...
 Slot 222092 | [HIT] | Q:9 | V in ctx:...-8320 is 964876. cryi...
 Slot 51084 | | Q: now | V in ctx:...i have now is there in ...
 Slot 94092 | [HIT] | Q:9 | V in ctx:...-8320 is 964876. cryi...
 Slot 28556 | | Q:0 | V in ctx:...cd05 is 075065. . no...
 Slot 29068 | [HIT] | Q:9 | V in ctx:...-8320 is 964876. cryi...

Output Token 3: '4'

--- FwPKM Layer 2 ---

Slot 121730 | [HIT] | Q:6 | V in ctx:...8320 is 964876. cryin...
 Slot 21378 | [HIT] | Q:6 | V in ctx:...8320 is 964876. cryin...
 Slot 54146 | [HIT] | Q:6 | V in ctx:...8320 is 964876. cryin...
 Slot 105858 | [HIT] | Q:6 | V in ctx:...8320 is 964876. cryin...
 Slot 63874 | [HIT] | Q:6 | V in ctx:...8320 is 964876. cryin...
 Slot 164738 | [HIT] | Q:6 | V in ctx:...8320 is 964876. cryin...
 Slot 121524 | [HIT] | Q:6 | V in ctx:...8320 is 964876. cryin...
 Slot 49538 | | (Empty)

--- FwPKM Layer 10 ---

Slot 139652 | [HIT] | Q:6 | V in ctx:...8320 is 964876. cryin...
 Slot 139398 | [HIT] | Q:6 | V in ctx:...8320 is 964876. cryin...
 Slot 98692 | | Q: . | V in ctx:...tention . there were a bu...
 Slot 139584 | [HIT] | Q:6 | V in ctx:...8320 is 964876. cryin...
 Slot 139747 | | Q:ups | V in ctx:...of pickups . i should ...
 Slot 139358 | [HIT] | Q:6 | V in ctx:...8320 is 964876. cryin...
 Slot 139479 | | Q:4 | V in ctx:...4884 is 543884. shara...
 Slot 139690 | [HIT] | Q:6 | V in ctx:...8320 is 964876. cryin...

Output Token 4: '8'

--- FwPKM Layer 2 ---

Slot 39146 | | Q: frown | V in ctx:...en frowned at the page ...
 Slot 103146 | [HIT] | Q:4 | V in ctx:...320 is 964876. crying...
 Slot 38939 | [HIT] | Q:4 | V in ctx:...320 is 964876. crying...
 Slot 39022 | [HIT] | Q:4 | V in ctx:...320 is 964876. crying...
 Slot 142058 | [HIT] | Q:4 | V in ctx:...320 is 964876. crying...
 Slot 39388 | [HIT] | Q:4 | V in ctx:...320 is 964876. crying...
 Slot 39266 | [HIT] | Q:4 | V in ctx:...320 is 964876. crying...
 Slot 102939 | [HIT] | Q:4 | V in ctx:...320 is 964876. crying...

--- FwPKM Layer 10 ---

Slot 249564 | [HIT] | Q:4 | V in ctx:...320 is 964876. crying...
 Slot 249364 | [HIT] | Q:4 | V in ctx:...320 is 964876. crying...
 Slot 153820 | | Q:3 | V in ctx:... 82382bed wall ...
 Slot 249607 | | Q:8 | V in ctx:...18 is 183863. going n...
 Slot 153620 | [HIT] | Q:4 | V in ctx:...320 is 964876. crying...
 Slot 153863 | | Q:1 | V in ctx:...4b is 859199. you wan...
 Slot 249413 | | Q: next | V in ctx:...right next to me , and ...
 Slot 249723 | | (Empty)

Output Token 5: '7'

--- FwPKM Layer 2 ---

Slot 209912 | [HIT] | Q:8 | V in ctx:...20 is 964876. crying ...
 Slot 104440 | [HIT] | Q:8 | V in ctx:...20 is 964876. crying ...
 Slot 215544 | [HIT] | Q:8 | V in ctx:...20 is 964876. crying ...
 Slot 209550 | [HIT] | Q:8 | V in ctx:...20 is 964876. crying ...
 Slot 190968 | [HIT] | Q:8 | V in ctx:...20 is 964876. crying ...
 Slot 104078 | [HIT] | Q:8 | V in ctx:...20 is 964876. crying ...
 Slot 215182 | [HIT] | Q:8 | V in ctx:...20 is 964876. crying ...
 Slot 49144 | [HIT] | Q:8 | V in ctx:...20 is 964876. crying ...

--- FwPKM Layer 10 ---

Slot 55559 | [HIT] | Q:8 | V in ctx:...20 is 964876. crying ...
 Slot 55515 | [HIT] | Q:8 | V in ctx:...20 is 964876. crying ...
 Slot 55603 | [HIT] | Q:8 | V in ctx:...20 is 964876. crying ...
 Slot 164103 | [HIT] | Q:8 | V in ctx:...20 is 964876. crying ...
 Slot 55782 | | Q: run | V in ctx:...ted to run away from here...
 Slot 71431 | | Q:8 | V in ctx:...4 is 818180. beloved ...
 Slot 55511 | | (Empty)
 Slot 164059 | | Q:9 | V in ctx:...b is 859199. you want...

Output Token 6: '6'

--- FwPKM Layer 2 ---

Slot 161835 | [HIT] | Q:7 | V in ctx:...0 is 964876. crying
 Slot 82475 | [HIT] | Q:7 | V in ctx:...0 is 964876. crying
 Slot 180779 | [HIT] | Q:7 | V in ctx:...0 is 964876. crying
 Slot 13867 | [HIT] | Q:7 | V in ctx:...0 is 964876. crying
 Slot 166443 | [HIT] | Q:7 | V in ctx:...0 is 964876. crying
 Slot 158251 | [HIT] | Q:7 | V in ctx:...0 is 964876. crying
 Slot 222251 | [HIT] | Q:7 | V in ctx:...0 is 964876. crying
 Slot 56875 | | Q:7 | V in ctx:... is 253297. through h...

--- FwPKM Layer 10 ---

Slot 141703 | | Q:ding | V in ctx:...s thudding against her ribs ...
 Slot 172935 | | Q: guys | V in ctx:...erous guys . wara froz...
 Slot 54663 | [HIT] | Q:7 | V in ctx:...0 is 964876. crying
 Slot 157063 | | Q: alive | V in ctx:...till alive . before th...
 Slot 141517 | | Q:3 | V in ctx:... is 158393. his legs ...
 Slot 172749 | [HIT] | Q:7 | V in ctx:...0 is 964876. crying
 Slot 54477 | [HIT] | Q:7 | V in ctx:...0 is 964876. crying
 Slot 71047 | | Q: . | V in ctx:...is place . i go here a...

Figure 7 | An example of FwPKM slot access of GDN+SWA | PKM@6+FwPKM@2, 10 during generating an NIAH-4K answer. The model memorizes the haystack for 3 extra iterations, i.e. 4-iter NIAH. See Section 5.1 for the visual elements' definitions.

Sakana AI's main research fields are evolution and collective intelligence of AI. The company's name is derived from the Japanese word さかな (sakana), which means fish. This represents the idea of a school of fish coming together and forming a coherent entity from simple rules, which is an analogy for collective intelligence. The company was founded by David Ha, Llion Jones and Ren Ito. Llion Jones co-authored the famous paper "Attention Is All You Need" when he was working for Google in 2017. The company raised \$30M in its seed funding round from Lux Capital and Khosla Ventures. The company raised approximately \$200M from companies such as Mitsubishi UFJ, SMBC, Mizuho, Itochu, KDDI, Nomura and Nvidia in its series A funding round in 2024. In January 2024, Sakana AI developed a method to build new AI models by breeding multiple existing models, which it sees as a means to democratize AI development, as this process does not require large computational resources. Sakana AI is also developing a model called the AI Scientist, which automates the entire process of scientific research. The Nikkei estimated the company's value at 19 billion yen in 2024.

Figure 8 | GDN+SWA|PKM@6+FwPKM@2, 10's FwPKM gating values on tokens from the Wikipedia article for Sakana AI. The blue color in the background denotes the gating intensity of the FwPKM at layer 2 and the red color denotes the FwPKM at layer 10. A darker color represents higher intensity. Black vertical lines show positions where FwPKM's fast weights are updated, which is every 32 tokens as we specified for this visualization example.

that indiscriminately caches recent history. In contrast, the higher-layer FwPKM exhibits highly selective activation.

Novelty detection As seen in Figure 8 (layer 10), gating values spike specifically for tokens related to rare named entities and proper nouns (e.g., "Sakana AI", "David Ha", "Llion Jones", and "Ren Ito"). This indicates that the model effectively distinguishes between general linguistic patterns (processed by slow weights) and novel, context-specific entities (processed by fast weights).

6. Cost Analyses

We evaluate the scalability and efficiency of FwPKM by profiling model size and computational costs, summarized in Table 1. Our analysis focuses on three key metrics:

- **Active Parameters:** The subset of parameters actually used during a forward pass, highlighting the architectural sparsity.
- **FLOPs (Floating Point Operations):** The theoretical computational volume required for each run.
- **FLOPS (FLOPs per Second):** The empirical hardware utilization efficiency, derived from actual running time.

Table 1 | Comparison of model size and computation cost. Active parameter counts reflect the sparse layer specifications: PKM utilizes 128 active rows, while FwPKM utilizes 8 active rows per token.

MODEL	Parameters (M)		FLOPs (T)	FLOPS (T/sec.)	Samples/sec.
	Total	Active			
GDN	112.11	112.11	22.04	150.00	54.44
PKM@2,6,10	509.08	106.62	20.92	112.19	42.90
FwPKM@2,6,10	519.12	116.48	22.74	54.12	19.04
PKM@6 + FwPKM@2,10	515.77	113.19	22.14	58.85	21.27
GDN+SWA	112.65	112.65	22.15	151.11	54.58
PKM@2,6,10	509.61	107.15	21.03	109.43	41.63
FwPKM@2,6,10	519.66	117.02	22.85	51.70	18.10
PKM@6 + FwPKM@2,10	516.31	113.73	22.24	58.55	21.06
GDN+FA	112.65	112.65	22.16	147.71	53.33
PKM@2,6,10	509.61	107.15	21.04	102.76	39.07
FwPKM@2,6,10	519.66	117.02	22.86	51.91	18.16
PKM@6 + FwPKM@2,10	516.31	113.73	22.25	57.69	20.74
FA	114.25	114.25	22.51	158.75	56.42
PKM@2,6,10	511.22	108.76	21.39	106.40	39.79
FwPKM@2,6,10	521.26	118.62	23.21	54.34	18.73
PKM@6 + FwPKM@2,10	517.91	115.33	22.60	61.80	21.87
GDN FwMLP@2,6,10	118.05	118.05	23.21	134.04	46.21
GDN+SWA FwMLP@2,6,10	118.58	118.58	23.31	128.40	44.06
GDN+FA FwMLP@2,6,10	118.58	118.58	23.32	97.18	33.33
FA FwMLP@2,6,10	120.19	120.19	23.67	118.85	40.16
LaCT	112.70	112.70	24.44	92.38	30.24

Profiling was conducted by running 100 training steps on a single H100 GPU with a global batch size of 8, using the configuration detailed in Section 4.1 and Appendix C.

Sparsity and Computational Volume Despite a substantial increase in total parameter count (approx. $5\times$ larger than baselines), the **Active Parameter** count of FwPKM models remains comparable to the dense baselines (e.g., GDN: 112M vs. FwPKM: 116M). Consequently, the theoretical computational cost (**FLOPs**) is remarkably efficient; in some cases, the sparsity of PKM/FwPKM makes them even less FLOPs-intensive than standard dense MLP layers.

Hardware Utilization and Kernels While theoretical costs are low, the wall-clock speed (**Samples per sec.**) and hardware utilization (**FLOPS**) reveal an implementation gap. FwPKM components currently run slower than their dense counterparts. This is primarily due to the maturity difference in kernel optimization: softmax attention and GDN benefit from highly optimized kernels like FlashAttention (Dao, 2024; Dao et al., 2022) and FlashLinearAttention (Yang and Zhang, 2024). In contrast, our sparse operations rely on less specialized implementations. Developing dedicated, hardware-aware kernels for sparse fast-weight updates is a critical future direction to bridge this gap and facilitate broader adoption.

7. Related Work

Softmax attention and linear variants Standard softmax attention has been foundational to the success of Transformers (Vaswani et al., 2017), fundamentally acting as a powerful form of asso-

ciative memory (Zhong et al., 2025). However, its quadratic complexity limits its application to extremely long sequences. To address this, various efficient architectures have been proposed. Linear attention (Katharopoulos et al., 2020) reduces complexity to linear time by changing the order of association. This direction includes Recurrent Neural Network (RNN) and State Space Model (SSM) evolutions such as Mamba (Gu and Dao, 2024) and Mamba2 (Dao and Gu, 2024), as well as specific variants like DeltaNet (Schlag et al., 2021b; Yang et al., 2024b), Gated DeltaNet (Yang et al., 2025), and RWKV7 (Peng et al., 2025). Other approaches like Memory Mosaics (Zhang and Bottou, 2025; Zhang et al., 2025a) improve softmax attention by techniques such as time-dimension smoothing and hierarchical memory design.

Fast weights and test-time training The concept of “fast weights” offers a powerful lens for unifying sequence modeling. Rooted in early work by Schmidhuber (1992) and Ba et al. (2016), this framework views linear transformers as fast weight programmers (Schlag et al., 2021a). Recently, this paradigm has been revitalized by Test-Time Training (TTT) (Sun et al., 2025; Zhang et al., 2025b) and Titans (Behrouz et al., 2025c), which explicitly update parameters during inference using gradient descent, enabling the model to memorize the current context. Theoretical frameworks like MIRAS (Behrouz et al., 2025a) and Test-Time Regression (Wang et al., 2025) unified various sequence models under the umbrella of test-time optimization and associative memory. These frameworks pointed out several directions for new model designs, namely memory architecture, memorization rule, memory retention rule, and optimizer. Our proposal of FwPKM contributes a novel memory architecture and a specific memorization rule accommodated for its structural sparsity.

Hybrid architectures Recognizing the complementary strengths of different sequence models, recent work has increasingly focused on hybrid architectures that combine the high-fidelity retrieval of quadratic attention with the efficiency of linear or recurrent layers. This includes hybrid models trained from scratch (Irie et al., 2025), as well as large-scale Hybrid LLMs such as Samba (Ren et al., 2025) and KimiLinear (Team et al., 2025). QwenNext (Qwen Team, 2025a,b) also employs this interleaved design. Furthermore, approaches like Artificial Hippocampus Networks (AHN, Fang et al. 2025) explore fine-tuning techniques to integrate these distinct memory systems effectively. Experiments in Section 4 demonstrated interactions between memories of different characteristics. The combination of linear attention (*i.e.* GDN), softmax attention, slow-weight sparse memory (*i.e.* PKM), and fast-weight sparse memory (*i.e.* FwPKM) implements a versatile memory system that excels at various tasks.

Memory models Beyond implicit knowledge in weights, explicit memory modules have been explored to enhance storage capacity. Early works include Memory Networks (Weston et al., 2015), while recent studies suggest even simple MLPs can function as memory (Csordás et al., 2023). To scale up capacity without prohibitive costs, sparse access mechanisms are essential. Product Key Memory (PKM, Berges et al. 2025; Lample et al. 2019) and PEER (He, 2024) utilize sparsity to access massive memory banks efficiently. Ultra Sparse Memory (Huang et al., 2025a,b) is a line of work that extends the PKM architecture with more expressive keys and other improvements. Our work builds upon the PKM structure but transitions it from a static “slow” memory to a dynamic “fast” memory.

Continual and episodic learning Finally, the ability to update memory parameters allows for continual learning and adaptation. Lin et al. (2025) showed that parameter-efficient fine-tuning of PKM effectively mitigates catastrophic forgetting. It demonstrated one dimension for continual learning – optimizing sparse slow weights via self-supervised learning to update semantic memory. FwPKM opens up the possibility for a different dimension of updating episodic memory by learning fast weights in an online learning manner. Nested Learning (Behrouz et al., 2025b) and TNT (Li et al., 2025) explored the direction of stacking multiple fast weight layers (*e.g.* Titans) and apply memory updates at varying frequencies. This “nested” memory structure enables gradually digesting changes in

faster weights into slower weights and exhibits strong performance. FwPKM maintains a huge memory bank and is updated at a low frequency to amortize optimization cost. It is a promising direction to design a hybrid memory system of varying-size FwPKMs and other memory components such as Titans with different optimization strategies as in Nested Learning (Behrouz et al., 2025b).

8. Conclusion

In this work, we introduced **Fast-weight Product Key Memory (FwPKM)**, a novel architecture that resolves the tension between memory capacity and computational efficiency in sequence modeling. By unifying the large-scale sparse storage of Product Key Memory (PKM) with the rapid adaptability of Test-Time Training (TTT), we transform PKM from a static retrieval module into a dynamic, context-responsive component. FwPKM performs *Sparse TTT* – updating key-value parameters online via sparse gradient descent – and enables models to efficiently memorize vast amounts of transient information and retrieve it thousands of tokens later.

Empirically, FwPKM demonstrates remarkable robustness. Models trained on short 4K-token sequences generalize effectively to 128K-token contexts (*i.e.* a 32× length extrapolation) without fine-tuning. Furthermore, we show that iterative reading exploits the TTT nature of FwPKM, boosting retrieval accuracy from < 10% to > 70% in difficult Needle-in-a-Haystack scenarios. Our ablation study and interpretability analyses confirm that FwPKM functions as a true episodic memory, selectively activating for novel entities and complementing the semantic knowledge stored in standard slow weights.

Despite these successes, challenges remain. The introduction of online updates introduces additional computational overhead, currently limited by the lack of optimized kernels for sparse updates. This motivates future systems work on hardware-aware sparse kernels to close the speed gap with dense baselines. On the modeling side, our continual learning experiments reveal that while FwPKM adapts rapidly, it struggles with long-term retention across domain shifts. Future research should focus on advanced retention mechanisms and memory consolidation strategies to prevent catastrophic forgetting of fast weights. Overall, FwPKM represents a promising step toward language models with versatile and mutually complementary memory systems.

Acknowledgments

We would like to thank Kai Arulkumaran, Luke Darlow, Stefania Druga, and the entire Sakana AI team for their insightful discussions and support throughout this project. We also extend our gratitude to Huayang Li, Qianying Liu, Richard Sproat, Yujin Tang, Qi Sun, and Stefano Peluchetti for their valuable feedback, which significantly strengthened the quality and clarity of this manuscript.

References

- Jimmy Ba, Geoffrey E. Hinton, Volodymyr Mnih, Joel Z. Leibo, and Catalin Ionescu. Using fast weights to attend to the recent past. In *NeurIPS*, 2016.
- Yushi Bai, Xin Lv, Jiajie Zhang, Hongchang Lyu, Jiankai Tang, Zhidian Huang, Zhengxiao Du, Xiao Liu, Aohan Zeng, Lei Hou, Yuxiao Dong, Jie Tang, and Juanzi Li. LongBench: A bilingual, multitask benchmark for long context understanding. In *ACL*, 2024.
- Ali Behrouz, Meisam Razaviyayn, Peilin Zhong, and Vahab Mirrokni. It’s all connected: A journey through test-time memorization, attentional bias, retention, and online optimization, 2025a. URL <https://arxiv.org/abs/2504.13173>.
- Ali Behrouz, Meisam Razaviyayn, Peilin Zhong, and Vahab Mirrokni. Nested learning: The illusion of deep learning architectures. In *NeurIPS*, 2025b. URL <https://openreview.net/forum?id=nbMeRvNb7A>.
- Ali Behrouz, Peilin Zhong, and Vahab Mirrokni. Titans: Learning to memorize at test time. In *NeurIPS*, 2025c. URL <https://openreview.net/forum?id=8GjSf9Rh7Z>.
- Vincent-Pierre Berges, Barlas Oguz, Daniel Haziza, Wen-tau Yih, Luke Zettlemoyer, and Gargi Ghosh. Memory layers at scale. In *ICML*, 2025.
- Jacob Buckman. LongCrawl64: A long-context natural-language dataset.
- Róbert Csordás, Kazuki Irie, and Jürgen Schmidhuber. Approximating two-layer feedforward networks for efficient Transformers. In *Findings of EMNLP*. Association for Computational Linguistics, 2023.
- Tri Dao. FlashAttention-2: Faster attention with better parallelism and work partitioning. In *ICLR*, 2024.
- Tri Dao and Albert Gu. Transformers are SSMS: Generalized models and efficient algorithms through structured state space duality. In *ICML*, 2024.
- Tri Dao, Daniel Y. Fu, Stefano Ermon, Atri Rudra, and Christopher Ré. FlashAttention: Fast and memory-efficient exact attention with IO-awareness. In *NeurIPS*, 2022.
- Yunhao Fang, Weihao Yu, Shu Zhong, Qinghao Ye, Xuehan Xiong, and Lai Wei. Artificial hippocampus networks for efficient long-context modeling, 2025. URL <https://arxiv.org/abs/2510.07318>.
- Leo Gao, Stella Biderman, Sid Black, Laurence Golding, Travis Hoppe, Charles Foster, Jason Phang, Horace He, Anish Thite, Noa Nabeshima, Shawn Presser, and Connor Leahy. The Pile: An 800gb dataset of diverse text for language modeling, 2020. URL <https://arxiv.org/abs/2101.00027>.
- Albert Gu and Tri Dao. Mamba: Linear-time sequence modeling with selective state spaces. In *COLM*, 2024. URL <https://openreview.net/forum?id=tEYskw1VY2>.
- Xu Owen He. Mixture of a million experts, 2024. URL <https://arxiv.org/abs/2407.04153>.
- Geoffrey E Hinton and David C Plaut. Using fast weights to deblur old memories. In *Proceedings of the Ninth Annual Conference of the Cognitive Science Society*, pages 177–186, 1987.

- Zihao Huang, Yu Bao, Qiyang Min, Siyan Chen, Ran Guo, Hongzhi Huang, Defa Zhu, Yutao Zeng, Banggu Wu, Xun Zhou, and Siyuan Qiao. UltraMemV2: Memory networks scaling to 120b parameters with superior long-context learning, 2025a. URL <https://arxiv.org/abs/2508.18756>.
- Zihao Huang, Qiyang Min, Hongzhi Huang, Yutao Zeng, Defa Zhu, Ran Guo, and Zhou Xun. Ultra-Sparse Memory Network. In *ICLR*, 2025b.
- Kazuki Irie, Morris Yau, and Samuel J. Gershman. Blending complementary memory systems in hybrid quadratic-linear Transformers. In *NeurIPS*, 2025.
- Keller Jordan, Yuchen Jin, Vlado Boza, Jiacheng You, Franz Cesista, Laker Newhouse, and Jeremy Bernstein. Muon: An optimizer for hidden layers in neural networks, 2024. URL <https://kellerjordan.github.io/posts/muon/>.
- Greg Kamradt. Needle In A Haystack – pressure testing LLMs, 2023. URL https://github.com/gkamradt/LLMTest_NeedleInAHaystack.
- Angelos Katharopoulos, Apoorv Vyas, Nikolaos Pappas, and François Fleuret. Transformers are RNNs: Fast autoregressive Transformers with linear attention. In *ICML*, volume 119 of *Proceedings of Machine Learning Research*, pages 5156–5165. PMLR, 2020.
- Guillaume Lample, Alexandre Sablayrolles, Marc’Aurelio Ranzato, Ludovic Denoyer, and Hervé Jégou. Large memory layers with product keys. In *NeurIPS*, 2019.
- Zeman Li, Ali Behrouz, Yuan Deng, Peilin Zhong, Praneeth Kacham, Mahdi Karami, Meisam Razaviyayn, and Vahab Mirrokni. TNT: Improving chunkwise training for test-time memorization, 2025. URL <https://arxiv.org/abs/2511.07343>.
- Jessy Lin, Luke Zettlemoyer, Gargi Ghosh, Wen-Tau Yih, Aram Markosyan, Vincent-Pierre Berges, and Barlas Oğuz. Continual learning via sparse memory finetuning, 2025. URL <https://arxiv.org/abs/2510.15103>.
- Calvin McCarter. Inverse distance weighting attention. *arXiv preprint arXiv:2310.18805*, 2023. URL <https://arxiv.org/abs/2310.18805>.
- Amirkeivan Mohtashami and Martin Jaggi. Landmark Attention: Random-access infinite context length for Transformers. In *NeurIPS*, 2023.
- Denis Paperno, Germán Kruszewski, Angeliki Lazaridou, Quan Ngoc Pham, Raffaella Bernardi, Sandro Pezzelle, Marco Baroni, Gemma Boleda, and Raquel Fernández. The LAMBADA dataset: Word prediction requiring a broad discourse context. In *ACL*. The Association for Computer Linguistics, 2016.
- Guilherme Penedo, Hynek Kydlíček, Loubna Ben Allal, Anton Lozhkov, Margaret Mitchell, Colin A. Raffel, Leandro von Werra, and Thomas Wolf. The FineWeb datasets: Decanting the web for the finest text data at scale. In *NeurIPS*, 2024.
- Bo Peng, Eric Alcaide, Quentin Anthony, Alon Albalak, Samuel Arcadinho, Stella Biderman, Huanqi Cao, Xin Cheng, Michael Chung, Leon Derczynski, Xingjian Du, Matteo Grella, Kranthi Kiran GV, Xuzheng He, Haowen Hou, Przemyslaw Kazienko, Jan Kocon, Jiaming Kong, Bartłomiej Koptyra, Hayden Lau, Jiaju Lin, Krishna Sri Ipsit Mantri, Ferdinand Mom, Atsushi Saito, Guangyu Song, Xiangru Tang, Johan S. Wind, Stanislaw Wozniak, Zhenyuan Zhang, Qinghua Zhou, Jian Zhu, and Rui-Jie Zhu. RWKV: Reinventing RNNs for the Transformer era. In Houda Bouamor, Juan Pino, and Kalika Bali, editors, *Findings of EMNLP*. Association for Computational Linguistics, 2023.

- Bo Peng, Ruichong Zhang, Daniel Goldstein, Eric Alcaide, Xingjian Du, Haowen Hou, Jiaju Lin, Jiaying Liu, Janna Lu, William Merrill, Guangyu Song, Kaifeng Tan, Saiteja Utpala, Nathan Wilce, Johan S. Wind, Tianyi Wu, Daniel Wuttke, and Christian Zhou-Zheng. RWKV-7 “Goose” with expressive dynamic state evolution. In *COLM*, 2025. URL <https://openreview.net/forum?id=ayB1PACN5j>.
- Bowen Peng, Jeffrey Quesnelle, Honglu Fan, and Enrico Shippole. YaRN: Efficient context window extension of large language models. In *ICLR*, 2024.
- Zihan Qiu, Zekun Wang, Bo Zheng, Zeyu Huang, Kaiyue Wen, Songlin Yang, Rui Men, Le Yu, Fei Huang, Suozhi Huang, Dayiheng Liu, Jingren Zhou, and Junyang Lin. Gated attention for large language models: Non-linearity, sparsity, and attention-sink-free. In *NeurIPS*, 2025. URL <https://openreview.net/forum?id=1b7wh04SfY>.
- Qwen Team. Qwen3-Next-80B-A3B-Thinking. <https://huggingface.co/Qwen/Qwen3-Next-80B-A3B-Thinking>, 2025a.
- Qwen Team. Qwen3 technical report, 2025b. URL <https://arxiv.org/abs/2505.09388>.
- Liliang Ren, Yang Liu, Yadong Lu, Yelong Shen, Chen Liang, and Weizhu Chen. Samba: Simple hybrid state space models for efficient unlimited context language modeling. In *ICLR*, 2025.
- Tim Salimans and Diederik P. Kingma. Weight normalization: A simple reparameterization to accelerate training of deep neural networks. In *NeurIPS*, 2016.
- Imanol Schlag, Kazuki Irie, and Jürgen Schmidhuber. Linear Transformers are secretly fast weight programmers. In Marina Meila and Tong Zhang, editors, *ICML*, volume 139 of *Proceedings of Machine Learning Research*, pages 9355–9366. PMLR, 2021a.
- Imanol Schlag, Tsendsuren Munkhdalai, and Jürgen Schmidhuber. Learning associative inference using fast weight memory. In *ICLR*, 2021b.
- Jürgen Schmidhuber. Learning to control fast-weight memories: An alternative to dynamic recurrent networks. *Neural Comput.*, 4(1):131–139, 1992.
- Noam Shazeer. GLU variants improve Transformer, 2020. URL <https://arxiv.org/abs/2002.05202>.
- Yu Sun, Xinhao Li, Karan Dalal, Jiarui Xu, Arjun Vikram, Genghan Zhang, Yann Dubois, Xinlei Chen, Xiaolong Wang, Sanmi Koyejo, Tatsunori Hashimoto, and Carlos Guestrin. Learning to (learn at test time): RNNs with expressive hidden states. In *ICML*, 2025.
- Kimi Team, Yu Zhang, Zongyu Lin, Xingcheng Yao, Jiayi Hu, Fanqing Meng, Chengyin Liu, Xin Men, Songlin Yang, Zhiyuan Li, Wentao Li, Enzhe Lu, Weizhou Liu, Yanru Chen, Weixin Xu, Longhui Yu, Yejie Wang, Yu Fan, Longguang Zhong, Enming Yuan, Dehao Zhang, Yizhi Zhang, T. Y. Liu, Haiming Wang, Shengjun Fang, Weiran He, Shaowei Liu, Yiwei Li, Jianlin Su, Jiezhong Qiu, Bo Pang, Junjie Yan, Zhejun Jiang, Weixiao Huang, Bohong Yin, Jiacheng You, Chu Wei, Zhengtao Wang, Chao Hong, Yutian Chen, Guanduo Chen, Yucheng Wang, Huabin Zheng, Feng Wang, Yibo Liu, Mengnan Dong, Zheng Zhang, Siyuan Pan, Wenhao Wu, Yuhao Wu, Longyu Guan, Jiawen Tao, Guohong Fu, Xinran Xu, Yuzhi Wang, Guokun Lai, Yuxin Wu, Xinyu Zhou, Zhilin Yang, and Yulun Du. Kimi Linear: An expressive, efficient attention architecture, 2025. URL <https://arxiv.org/abs/2510.26692>.
- Ashish Vaswani, Noam Shazeer, Niki Parmar, Jakob Uszkoreit, Llion Jones, Aidan N. Gomez, Lukasz Kaiser, and Illia Polosukhin. Attention is all you need. In *NeurIPS*, 2017.

- Ke Alexander Wang, Jiaxin Shi, and Emily B. Fox. Test-time regression: A unifying framework for designing sequence models with associative memory, 2025. URL <https://arxiv.org/abs/2501.12352>.
- Maurice Weber, Daniel Y. Fu, Quentin Anthony, Yonatan Oren, Shane Adams, Anton Alexandrov, Xiaozhong Lyu, Huu Nguyen, Xiaozhe Yao, Virginia Adams, Ben Athiwaratkun, Rahul Chalamala, Kezhen Chen, Max Ryabinin, Tri Dao, Percy Liang, Christopher Ré, Irina Rish, and Ce Zhang. RedPajama: An open dataset for training large language models. In *NeurIPS*, 2024.
- Jason Weston, Sumit Chopra, and Antoine Bordes. Memory networks. In *ICLR*, 2015.
- Songlin Yang and Yu Zhang. FLA: A Triton-based library for hardware-efficient implementations of linear attention mechanism, January 2024. URL <https://github.com/fla-org/flash-linear-attention>.
- Songlin Yang, Bailin Wang, Yikang Shen, Rameswar Panda, and Yoon Kim. Gated linear attention Transformers with hardware-efficient training. In *ICML*, 2024a.
- Songlin Yang, Bailin Wang, Yu Zhang, Yikang Shen, and Yoon Kim. Parallelizing linear Transformers with the delta rule over sequence length. In *NeurIPS*, 2024b.
- Songlin Yang, Jan Kautz, and Ali Hatamizadeh. Gated delta networks: Improving Mamba2 with delta rule. In *ICLR*, 2025.
- Jianyu Zhang and Leon Bottou. Memory mosaics at scale. In *NeurIPS*, 2025. URL <https://openreview.net/forum?id=IfD2MKTmWv>.
- Jianyu Zhang, Niklas Nolte, Ranajoy Sadhukhan, Beidi Chen, and Léon Bottou. Memory mosaics. In *ICLR*, 2025a.
- Tianyuan Zhang, Sai Bi, Yicong Hong, Kai Zhang, Fujun Luan, Songlin Yang, Kalyan Sunkavalli, William T. Freeman, and Hao Tan. Test-time training done right, 2025b. URL <https://arxiv.org/abs/2505.23884>.
- Shu Zhong, Mingyu Xu, Tenglong Ao, and Guang Shi. Understanding Transformer from the perspective of associative memory, 2025. URL <https://arxiv.org/abs/2505.19488>.

A. FwPKM Implementation Details

A.1. Lookahead Value Targets

By default, FwPKM pairs each query \mathbf{q}_t with the value computed from the same token, \mathbf{v}_t , in the memorization loss (Eq. 13). However, next-token prediction benefits more directly from information about *future* tokens. We therefore use a **lookahead** construction that pairs \mathbf{q}_t with the next token’s value \mathbf{v}_{t+1} when applying chunk-level updates.

Concretely, we keep the retrieval definition $\hat{\mathbf{v}}_t = \text{PKM}(\mathbf{q}_t; \theta)$ unchanged, and only shift the target value in the memorization objective. We use gradients from this new objective to update fast-weight value matrix V .

$$\mathcal{L}_{\text{mem}}^{\text{LA}} = \sum_{t=1}^{C-1} \frac{1}{2} g_t \|\mathbf{v}_{t+1} - \hat{\mathbf{v}}_t\|_2^2. \quad (19)$$

Intuitively, this encourages FwPKM to store information that is immediately useful for predicting the next token, similar in spirit to using short convolutions in linear-attention variants (Gu and Dao, 2024; Peng et al., 2023; Yang et al., 2024a).

Importantly, we apply the fast-weight update only after processing the entire chunk, so lookahead targets do not affect predictions within the same chunk. We carefully handle values at chunk boundaries. For efficiency, we drop the last predicted value in each chunk for efficiency *at training time* (which results in dropping 8 tokens for a 4096-token training sequence). At inference time, a FwPKM maintains a value cache that accumulates new $(\mathbf{v}_{t+1}, \hat{\mathbf{v}}_t)$ pairs. When a pre-defined update chunk size is reached (e.g. 512 in PPL evaluation, haystack length in NIAH evaluation), FwPKM consumes stored pairs to update its fast weights.

In our experiments, lookahead targets improved performance and we use it as the default unless otherwise noted.

A.2. Inverse-Distance Weighting (IDW) Scoring

A query–key score in PKM is typically the dot product $s_i = \mathbf{q}^\top \mathbf{K}_i$. However, a key row can increase its score by growing its magnitude, without necessarily being *close* to the query in representation space. We therefore consider inverse distance weighting (IDW, McCarter 2023) as a drop-in alternative scoring function:

$$s_i^{\text{IDW}} = -\log(\epsilon + \|\mathbf{q} - \mathbf{K}_i\|_2^2), \quad (20)$$

where we use $\epsilon = 10^{-3}$. Due to the use of Euclidean distance, gradients produced by IDW scores push keys to behave as *prototypes*—centroids of query clusters. We apply IDW by replacing only the query–key scoring function inside PKM’s Top- k selection (for each sub-key set in product-key retrieval); all other steps of PKM retrieval remain unchanged. Empirically, we found IDW scoring to yield better performance than dot-product scoring in our FwPKM setup.

A.3. Target Normalization and Gradient Clipping

We z-score normalize target values \mathbf{v}_t along the feature dimension to stabilize optimization. Unlike standard slow-weight training, we do not clip gradients for fast-weight updates; this helps FwPKM match the scale of unbounded target values.

A.4. Loss Reduction and Effective Step Size

In Eq. 13 we sum over tokens and features. We avoid mean reduction so that the update magnitude does not shrink with chunk size C or value dimension d_v . Concretely, if one uses mean reduction over (t, j) , the gradient of an element $V_{i,j}$ scales by $1/(Cd_v)$, which effectively changes the fast-weight step size.

A.5. Gating-weighted Memorization

We weight each per-token MSE by g_t in Eq. 13. Intuitively, g_t measures how much the model relies on the memory output at this position, so it also serves as a natural importance weight for deciding which tokens should write more strongly. Note that we use gate g_t both to interpolate outputs (Eq. 12) and to weight memorization updates in \mathcal{L}_{mem} (and $\mathcal{L}_{\text{mem}}^{\text{LA}}$).

B. Pseudo Code

Algorithm 1: Fast-weight Product Key Memory (FwPKM) Processing

Input : Hidden states $\mathbf{h}_{1:T} \in \mathbb{R}^{T \times d}$,
Fast weights $\theta = \{V \in \mathbb{R}^{N \times d_v}, K^{(1)}, K^{(2)} \in \mathbb{R}^{\sqrt{N} \times d_k/2}\}$,
Slow weights ϕ

Hyperparameters: Chunk size C , Key dim d_k , Value dim d_v , Top-K k

Output : Output sequence $\mathbf{o}_{1:T} \in \mathbb{R}^{T \times d_v}$

```

1 for  $t = 1$  to  $T$  step  $C$  do
  // -- Phase 1: Forward Pass (Inference) --
2   $\mathbf{h}_{\text{chunk}} \leftarrow \mathbf{h}_{t:t+C}$  // Shape: (C, d)
  // Compute projections using Slow Weights  $\phi$ 
3   $\mathbf{q} \leftarrow \text{Linear}_{\phi}^q(\text{RMSNorm}_{\phi}^q(\mathbf{h}_{\text{chunk}}))$  // Shape: (C,  $d_k$ )
4   $\mathbf{v} \leftarrow \text{Linear}_{\phi}^v(\text{RMSNorm}_{\phi}^v(\mathbf{h}_{\text{chunk}}))$  // Shape: (C,  $d_v$ )
5   $g \leftarrow \sigma(\text{Linear}_{\phi}^g(\text{RMSNorm}_{\phi}^g(\mathbf{h}_{\text{chunk}})))$  // Shape: (C, 1)
  // Split query into two halves for Product Keys
6   $\mathbf{q}^{(1)}, \mathbf{q}^{(2)} \leftarrow \text{Split}(\mathbf{q})$  // Shapes: (C,  $d_k/2$ )
  // Sparse Retrieval (PKM) with current Fast Weights
7  for  $m \in \{1, 2\}$  do
  // IDW Scoring
8   $s^{(m)} \leftarrow -\log(10^{-3} + \|\mathbf{q}^{(m)} - K^{(m)}\|_2^2)$  // Shape: (C,  $\sqrt{N}$ )
  // Top-k Indices
9   $\mathcal{I}^{(m)} \leftarrow \text{Top-k}(s^{(m)})$  // Shape: (C,  $k$ )
  // Select final Top-k from the  $k \times k$  restricted product
10  $S_{\text{target}} \leftarrow \{s_i^{(1)} + s_j^{(2)} \mid (i, j) \in \mathcal{I}^{(1)} \times \mathcal{I}^{(2)}\}$  //  $k^2$  candidates per token
11  $\mathcal{I} \leftarrow \text{Top-k}(S_{\text{target}})$  // Final  $k$  indices per token
12  $\hat{\mathbf{v}} \leftarrow \sum_{(i,j) \in \mathcal{I}} \text{softmax}(S_{\text{target}})_{(i,j)} V_{\text{flat-idx}(i,j)}$  // Shape: (C,  $d_v$ )
  // Gated Residual Output
13  $\mathbf{o}_{\text{chunk}} \leftarrow g \cdot \hat{\mathbf{v}} + (1 - g) \cdot \mathbf{v}$  // Shape: (C,  $d_v$ )

  // -- Phase 2: Backward Pass for Memorization --
14  $\mathbf{v}_{\text{target}} \leftarrow \text{Shift}(\mathbf{v}, +1)$  // Lookahead Target:  $\mathbf{v}_{t+1}$ 
15  $\mathcal{L}_{\text{mem}}^{\text{LA}} \leftarrow \sum_{\text{step}=1}^{C-1} \frac{1}{2} g_{\text{step}} \|\mathbf{v}_{\text{target}} - \hat{\mathbf{v}}_{\text{step}}\|_2^2$ 
16  $\nabla_{V_i}^{\text{agg}} \leftarrow \frac{1}{N_i^{\text{read}}} \nabla_{V_i} \mathcal{L}_{\text{mem}}$  // Aggregate gradients by slot usage
17  $V \leftarrow V - \nabla_V^{\text{agg}}$  // Update Values

  // -- Phase 3: Backward Pass for Addressing (Anti-collapsing) --
18 for  $m \in \{1, 2\}$  do
19  $\bar{p}^{(m)} \leftarrow \text{AvgSlotUsage}(\mathcal{I}^{(m)}, \text{chunk})$  // Shape: ( $\sqrt{N}$ ,)
20  $\mathcal{L}_{\text{addr}}^{(m)} \leftarrow -H(\bar{p}^{(m)})$  // Maximize Entropy
21  $K^{(m)} \leftarrow K^{(m)} - \nabla_{K^{(m)}} \mathcal{L}_{\text{addr}}^{(m)}$  // Update Keys
22 return  $\mathbf{o}_{1:T}$ 

```

et al., 2024), and we found SGD with momentum achieves lower training PPL in our experiments. LaCT uses data-dependent learning rate and L2 weight normalization to improve memorization and retention. We compared several configurations of sliding window size (W) and update chunk size (C). Among $512C + 512W$, $512C + 2048W$, $512C + 4096W$, and $2048C + 2048W$, the best model is $512C + 2048W$.

One notable difference between LaCT (or more generally TTT) and FwMLP/FwPKM is that LaCT/TTT maintains an individual set of fast weights for each sequence in a mini batch, while FwMLP/FwPKM uses a shared set of fast weights for all sequences.

D. Ablation Study

To understand the influence of techniques proposed in Section 3, we conduct ablation experiments based on the GDN+SWA | PKM6+FwPKM@2,10 model. The following variants are trained and evaluated using the same pipelines.

- “w/ 1 head \times Top-32” uses a different Top- K setting as the name suggests.
- “w/ 4 heads \times Top-8” uses a different multi-head setting as the name suggests.
- “w/o value norm” does NOT z-score normalize target values.
- “w/o addr loss” does NOT use the marginal entropy loss to update key matrices, instead it uses the MSE loss to update both the keys and value matrices.
- “w/o gating” does NOT use g_t .
- “w/o loss weight” uses g_t but does NOT weight MSE loss with it.
- “w/o lookahead” does NOT use lookahead values as MSE targets.

In addition, we found that replacing IDW score with dot-product score often results in memory collapsing and loss divergence so do not include it in the ablation study.

D.1. Evaluation

As shown in Figures 9, 10, 11, 12, and 13, we conduct the same evaluation experiments from Section 4 to ablated models. a) Notably, removing lookahead values yields the most significant harm to model performance. Many techniques bring slight PPL improvement, but lead to less healthy memory utility and subsequently worse NIAH accuracies to different extents. b) Addressing loss and weighting MSE loss with gating values are important for NIAH retrieval accuracy. c) A larger effective top- k slightly improves performance in some tasks, but the default setting of 1 head \times 8 slots strikes a sweet spot between task performance and compute efficiency (See computation cost of ablated models in Table 3).

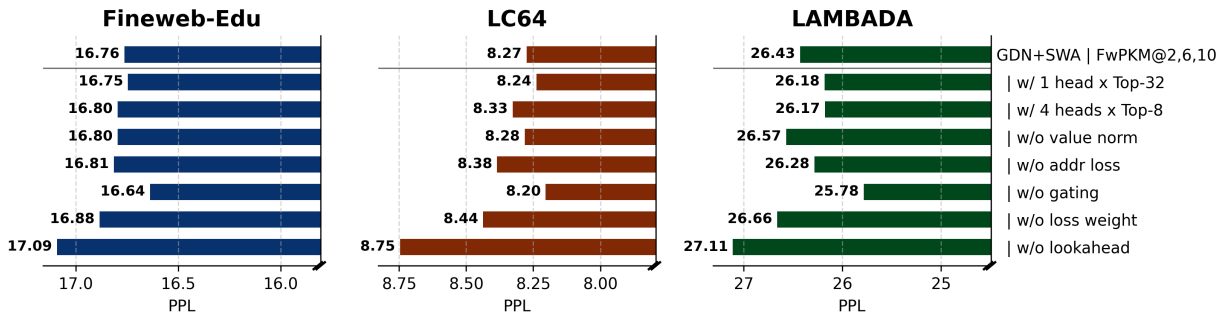


Figure 9 | Ablation study: Perplexity on Fineweb-Edu, LC64, and LAMBADA. We use bar colors to help distinguish between models with different types of memory components.

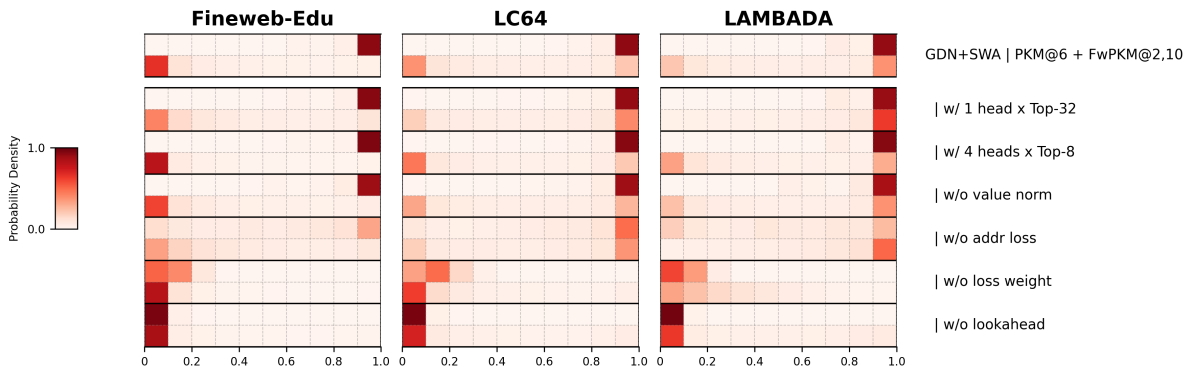


Figure 10 | Ablation study: FwPKM gating value distribution on Fineweb-Edu, LC64, and LAMBADA test sets. Each row represents one FwPKM layer. The probability densities are categorized into 10 bins. A darker color suggests a higher probability density of a bin.

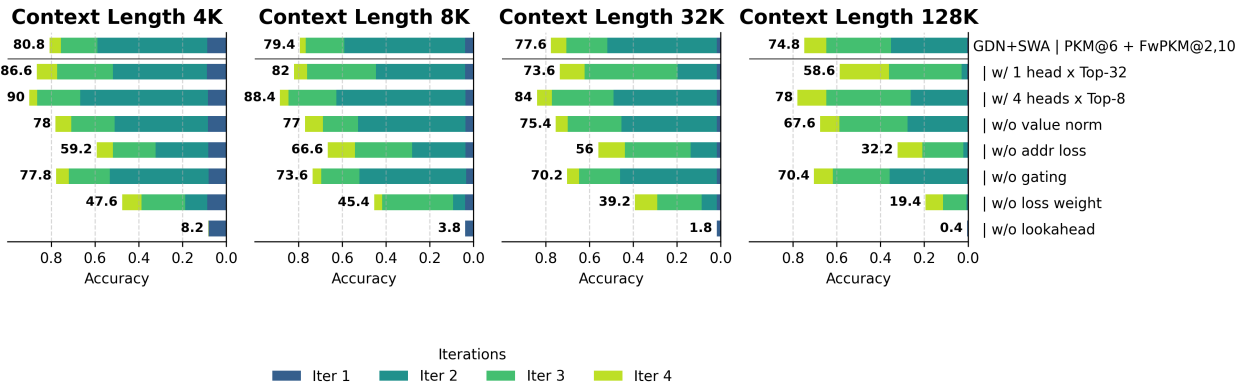


Figure 11 | Ablation study: Stacked bar plots for NIAH accuracy results on 4K-/8K-/32K-/128K-length test sets. Each stacked bar shows the accuracies of {1, 2, 3, 4}-iter NIAH evaluations.

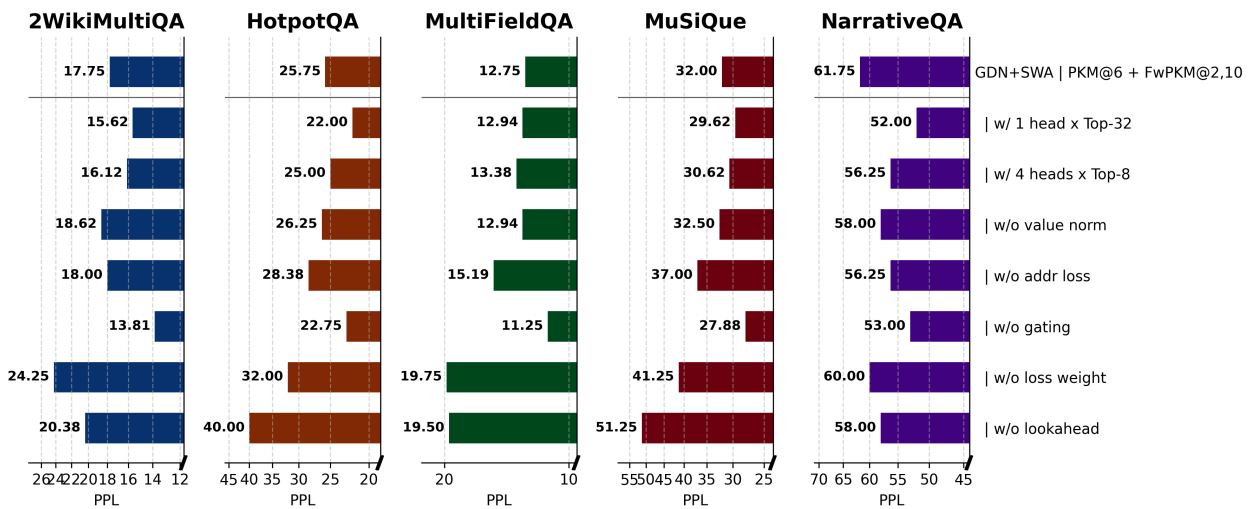


Figure 12 | Ablation study: Perplexity on five Longbench tasks. We use bar colors to help distinguish between models with different types of memory components.

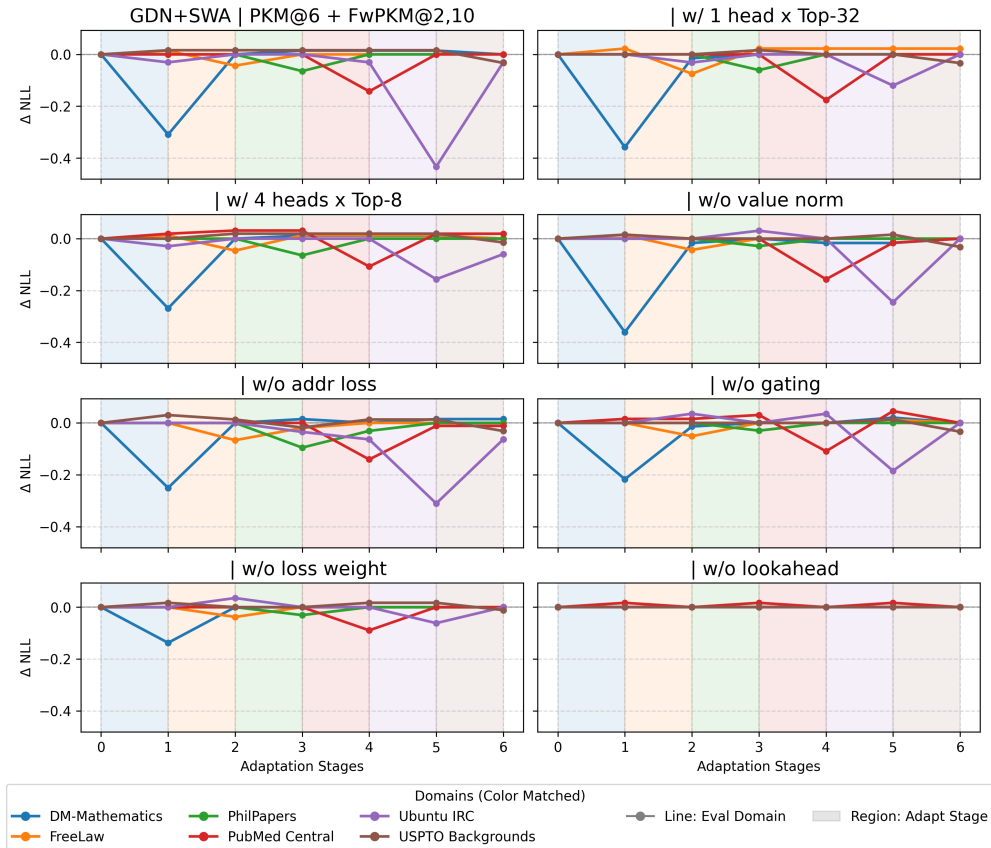


Figure 13 | Ablation study: Change of negative log-likelihood (ΔNLL) on six Pile domain datasets before and after 6 adaptation stages of test-time learning on each domain dataset.

Table 3 | Ablation study: Comparison of model size and computation cost.

MODEL	Parameters (M)		FLOPs (T)	FLOPS (T/sec.)	Samples/sec.
	Total	Active			
GDN+SWA PKM@6 + FwPKM@2,10	516.31	113.73	22.24	58.55	21.06
w/ 1 head x Top-32	516.31	113.76	22.24	58.28	20.96
w/ 4 heads x Top-8	520.24	117.69	22.71	48.47	17.08
w/o value norm	516.31	113.73	22.24	65.03	23.39
w/o addr loss	516.31	113.73	22.24	65.91	23.70
w/o gating	516.30	113.72	22.24	61.30	22.05
w/o loss weight	516.31	113.73	22.24	61.06	21.96
w/o lookahead	516.31	113.73	22.24	58.70	21.11

D.2. Freezing Fast Weights

To consolidate the evidence that FwPKM contributes to long-context language modeling, we conduct extra PPL evaluation experiments as in Section 4.2 but *freezing* FwPKM’s fast-weight parameters (*i.e.* value matrix V and key matrices $K^{(1)}, K^{(2)}$). Figure 14 shows that freezing fast weights significantly increase perplexity on long-context datasets LC64 and LAMBADA while Fineweb-Edu is less affected, further supporting conclusions in Section 4.2.

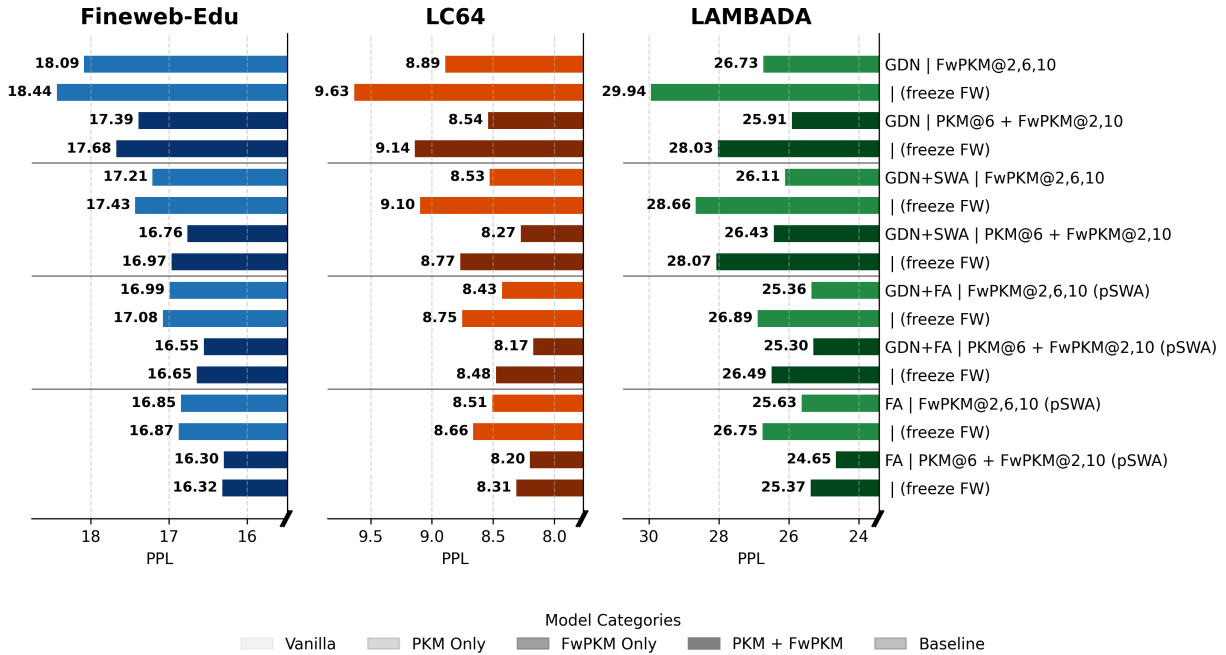


Figure 14 | Ablation study: Perplexity on Fineweb-Edu, LC64, and LAMBADA. Unlike previous experiments, the fast-weight parameters in FwPKM are frozen. We use bar colors to help distinguish between models with different types of memory components.

D.3. Addressing Metrics

The design choices have different impact on the evenness of slot usage, and we use three addressing metrics to characterize it. Recall that we define N_i^{read} to be the “row contribution”, *i.e.* the number of times a value row V_i is accessed.

- **Collision rate** is the ratio of *competitive* slot accesses: $\sum_{N_i^{\text{read}} > 1} N_i^{\text{read}} / N^{\text{total}}$, where N^{total} is the total number of slot accesses.
- **Coverage rate** is the ratio of accessed slots: $\sum_{N_i^{\text{read}} > 0} 1 / N$.
- **KLD** is the Kullback–Leibler divergence between the average slot use distribution and an uniform distribution:

$$p_i^{\text{read}} = N_i^{\text{read}} / \sum_i N_i^{\text{read}}$$

$$\text{KLD} = \sum_i p_i^{\text{read}} \log \frac{p_i^{\text{read}}}{1/N}.$$

For each evaluation dataset and each metric, we calculate the metric every 32K tokens, which gives us $8\text{M} / 32\text{K} = 256$ numbers and we take their average. We choose 32K tokens because a GDN+SWA | PKM@6+FwPKM@2, 10 model selects 8 slots per token and perfectly balanced slot selection would cover $32\text{K} \times 8 = 256\text{K}$ slots, which is the exact number of FwPKM slots. We report the metrics averaged across two FwPKM layers.

As shown in Table 4, memory slot use is more balanced on long-context datasets LAMBADA and LC64 but still far from uniform distribution. Increasing head number or Top-K can improve the evenness but also increases collision rate. Ablating the addressing loss leads to a concentrated slot access pattern.

Unhealthy slot access statistics such as in the “w/o addr loss” model are paired with degraded performance in certain tasks (*e.g.* NIAH). If we compare models of effectively Top-32 slot activations (*i.e.* “w/ 1 head x Top-32” and “w/ 4 heads x Top-8”) against models of effectively Top-8 slot activations, despite the former group having higher coverage and lower KLD, their differences in evaluation experiments (Figures 9, 10, 11, 12, and 13) do not correlate with the difference in slot access statistics. The results might be affected by compound factors such as the Top- k mechanism per se, but we believe it is important to mitigate severely unbalanced memory slot access, for example by minimizing the addressing loss.

Table 4 | Memory addressing metrics. Coll. – collision rate (%). Cov. – coverage rate (%). KLD – KLD against uniform distribution. Darker colors indicate better performance (*i.e.* low collision, high coverage, low KLD).

Model	Fineweb-Edu			LAMBADA			LC64		
	Coll. ↓	Cov. ↑	KLD ↓	Coll. ↓	Cov. ↑	KLD ↓	Coll. ↓	Cov. ↑	KLD ↓
GDN+SWA PKM@6 + FwPKM@2,10	55.7	15.8	2.2	83.1	32.1	1.9	85.2	28.4	2.1
w/ 1 head x Top-32	78.1	41.7	1.3	95.3	64.1	1.3	95.4	55.0	1.9
w/ 4 heads x Top-8	78.2	41.4	1.4	95.5	60.8	1.4	95.3	60.9	1.7
w/o value norm	55.6	15.8	2.2	83.1	32.1	1.8	84.9	28.9	2.1
w/o addr loss	84.6	7.2	3.6	94.9	12.0	3.9	96.4	8.0	5.4
w/o gating	55.2	16.0	2.2	83.1	32.1	1.9	84.3	29.9	2.0
w/o loss weight	57.3	15.5	2.2	83.8	31.2	1.9	85.6	28.1	2.1
w/o lookahead	52.5	16.6	2.1	82.4	33.1	1.8	82.5	32.8	1.8

E. More Visualization Examples

E.1. Improving Perplexity over Sequence Boundary

In long-context datasets LC64 and LAMBADA, a document can span over multiple 4K-token sequences. The ability of carrying over memory states across sequence boundaries makes FwPKM models excel at reducing the PPL of tokens that require cross-sequence dependency.

In Figure 15, we demonstrate the advantage of FwPKM models ($*|PKM@6+FwPKM@2,10$) by showing their PPL reduction from vanilla counterparts (GDN, GDN+SWA, GDN+FA) on the first ten LC64 documents used in Section 4.2. Within each document, we calculate the average of PPLs cumulated from the beginning of the document. Then we plot the reduction of cumulative PPL every 128 tokens. The orange lines denote the cumulative PPL difference between $*|PKM@6+FwPKM@2,10$ and their vanilla counterparts, and the blue lines show the PPL difference between $*|PKM@2,6,10$ and vanilla counterparts as reference.

While the PKM-only variants show significant PPL reduction over the vanilla models, the PPL reduction curves are relatively smooth, suggesting constant advantage throughout each document. On the other hand, the FwPKM models have more jagged curves. We hypothesize that these ‘‘PPL drops’’ are caused by FwPKM exploiting information from previous sequences, which is impossible for the vanilla and PKM-only models.

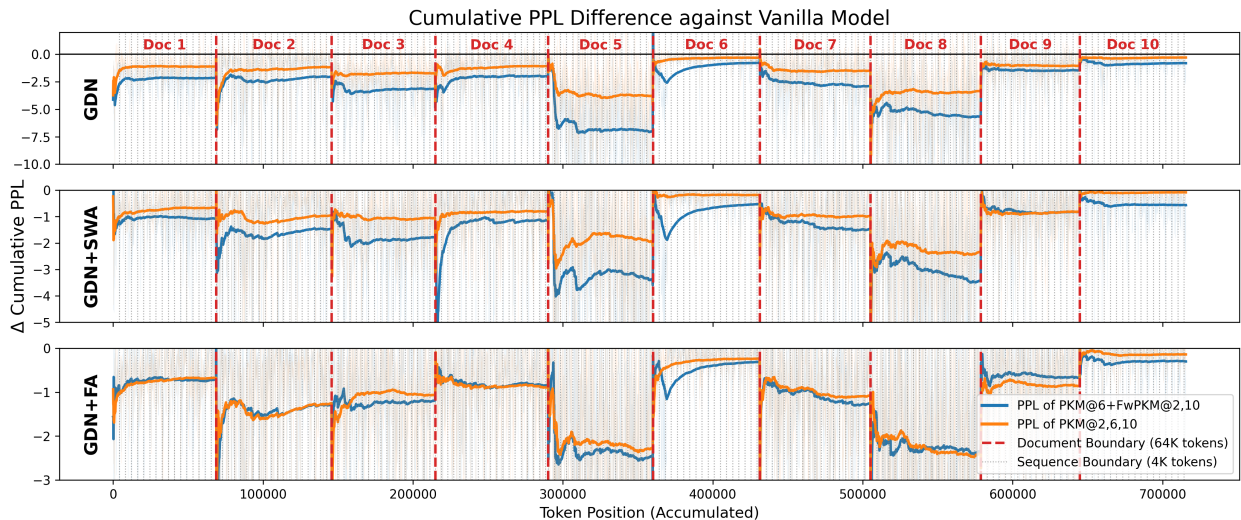


Figure 15 | PPL reduction of $*|PKM@6+FwPKM@2,10$ and $*|PKM@2,6,10$ from vanilla GDN, GDN+SWA, and GDN+FA models at different token positions.

E.2. Extra Selective Gating Example

Figure 16 shows the token-level FwPKM gating values for the Introduction section of this paper.

Long-context language modeling often requires remembering specific, local facts (e.g., a name, a variable binding, a constraint) introduced tens of thousands of tokens earlier, and retrieving them when needed. The core sequence modeling layers, or token mixers, can be viewed as associative memory systems (Behrouz et al., 2025c; Dao and Gu, 2024; Gu and Dao, 2024; Peng et al., 2025; Sun et al., 2025; Vaswani et al., 2017; Yang et al., 2024b, 2025). In this framework, information from past tokens is encoded into storage (i.e., the process of memorization) and later integrated into a prediction step by querying that storage (i.e., the process of retrieval).

The current landscape is defined by a trade-off between memory capacity and computational efficiency. Softmax self-attention (Vaswani et al., 2017; Zhong et al., 2025) memorizes by explicitly storing a key-value pair for every past token and retrieves by comparing the current query to all stored keys, producing a weighted sum of values. This yields high-fidelity retrieval but at quadratic cost with sequence length. In contrast, modern Recurrent Neural Networks (RNNs) such as linear attention (Katharopoulos et al., 2020), Mamba 2 (Dao and Gu, 2024), and DeltaNet (Schlag et al., 2021a; Yang et al., 2024b) compress history into a fixed-size state using learned update rules (e.g., Hebbian-style accumulation or Delta-rule error correction) and retrieve via a state readout in the form of vector-matrix multiplication. While this enables efficient, sub-quadratic retrieval, the fixed state capacity inherently limits the depth of information the model can retain compared to softmax attention.

To address the capacity limitations of these modern RNNs, recent work on Test-Time Training (TTT, Sun et al., 2025; Zhang et al., 2025b) and Titans (Behrouz et al., 2025c) replaces the fixed state matrix with a “fast weight” (Hinton and Plaut, 1987; Schmidhuber, 1992) neural network (typically an MLP). Similar to a state matrix, this MLP adapts to input sequences on-the-fly by minimizing a reconstruction loss. However, these approaches face a scaling bottleneck: dense network structure. An MLP’s computation scales linearly with its parameter count. To store the massive amount of information required for long-context tasks, the fast-weight MLP must be large; yet, updating and querying a large, dense MLP frequently is computationally infeasible.

Figure 16 | GDN+SWA|PKM@6+FwPKM@2, 10’s FwPKM gating values on tokens from the Introduction section. The blue color in the background denotes the gating intensity of the FwPKM at layer 2 and the red color denotes the FwPKM at layer 10. A darker color represents higher intensity. Black vertical lines show positions where FwPKM’s fast weights are updated, which is every 32 tokens as we specified for this visualization example.